Practical Use of the Ubiquitous-Joint Constitutive Model for the Simulation of Anisotropic Rock Masses

B. L. Sainsbury & D. P. Sainsbury

Rock Mechanics and Rock Engineering

ISSN 0723-2632
Volume 50
Number 6

Rock Mech Rock Eng (2017)
50:1507-1528
DOI 10.1007/s00603-017-1177-3

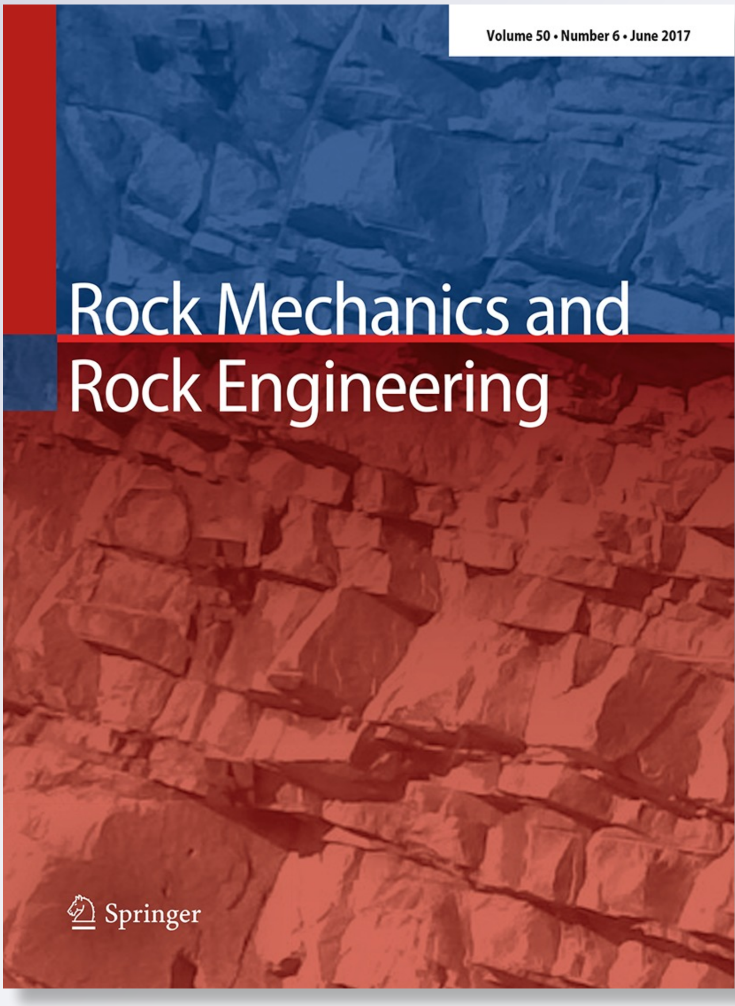

Springer

Rock Mech Rock Eng (2017) 50:1507–1528
DOI 10.1007/s00603-017-1177-3

ORIGINAL PAPER

Practical Use of the Ubiquitous-Joint Constitutive Model for the Simulation of Anisotropic Rock Masses

B. L. Sainsbury[1] · **D. P. Sainsbury**[1,2]

Received: 17 August 2016 / Accepted: 23 January 2017 / Published online: 3 February 2017

Abstract Anisotropic rock masses, the behavior of which is dominated by closely spaced planes of weakness, present particular difficulties in rock engineering analyses. The orientation of discontinuities relative to an excavation face has a significant influence on the behavioral response. At the present time, discontinuum modeling techniques provide the most rigorous analyses of the deformation and failure processes of anisotropic rock masses. However, due to their computational efficiency continuum analyses are routinely used to represent laminated materials through the implementation of a Ubiquitous-Joint model. The problem with Ubiquitous-Joint models is that they do not consider the effects of joint spacing, length and stiffness. As such, without an understanding of the limitations of the modeling approach and detailed calibration of the material response, simulation results can be misleading. This paper provides a framework to select and validate ubiquitous-joint constitutive properties.

Keywords Anisotropic · Ubiquitous-joint · Subiquitous · Numerical simulation · Discontinuum

1 Introduction

The strength and deformation behavior of a rock mass is governed strongly by (a) the 'intact' strength of the rock blocks and (b) the presence of planes of weakness such as joints, bedding, foliation and other discontinuities. Anisotropic rock mass strength and deformation behavior is usually observed when a significant portion of the discontinuities is aligned in a preferred direction, such as the shale rock masses illustrated in Fig. 1.

Various discontinuum modeling techniques are available that explicitly simulate joints and discontinuities within an anisotropic rock mass. However, due to the computational intensity of these numerical techniques, it is not practical to explicitly simulate the joint fabric of an entire rock mass for routine analyses of large-scale excavations (Riahi and Curran 2008; Karampinos et al. 2015). To overcome these computational limitations, the continuum-based Ubiquitous-Joint constitutive model is commonly used to represent anisotropic and foliated rock masses (Board et al. 1996; Clark 2006; Leitner et al. 2006; Sainsbury et al. 2008).

At the present time, there are no established guidelines for assigning material properties for the Ubiquitous-Joint model. A common misconception is that the material properties (matrix and joints) are comparable with the explicit block and joint description used in typical discontinuum analyses (Leitner et al. 2006). As demonstrated herein, the selection of matrix and joint properties based on a direct input of the measured block and joint strength will result in a material response that does not represent the true rock mass strength or deformation profile. This variation occurs since the Ubiquitous-Joint model does not consider the effects of joint spacing and joint stiffness. As a result of this, calibration of a Ubiquitous-Joint model response is required to provide meaningful modeling results for engineering design.

✉ B. L. Sainsbury
bre-anne.sainsbury@monash.edu

1 Department of Civil Engineering, Monash University, Clayton 3800, Australia

2 NOMA-Consulting, Melbourne 3000, Australia

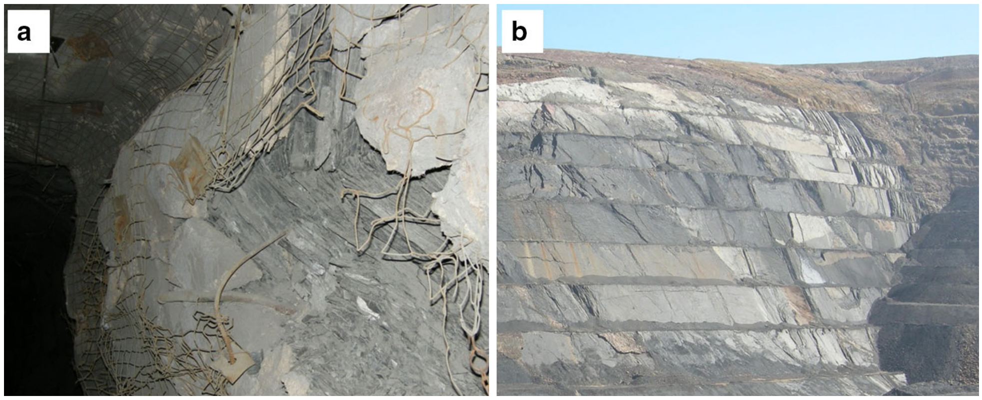

Fig. 1 Examples of anisotropic rock masses; **a** buckling of shale bedding in an underground drive, **b** slope angle controlled by shale bedding planes in an open pit slope

2 Background

2.1 The Ubiquitous-Joint and Subiquitous Constitutive Models

The Ubiquitous-Joint model corresponds to a Mohr–Coulomb material that exhibits a well-defined strength anisotropy due to embedded planes of weakness. As shown in Fig. 2, the planes of weakness can be assigned different orientations for each zone in the model. The criterion for failure on the plane of weakness consists of a composite Mohr–Coulomb envelope with a tension cutoff. The zone-based matrix and joint properties (as outlined in Fig. 2) must be specified within the model.

The formulation of the Ubiquitous-Joint model assumes a direction of weakness with no associated spacing or length. The bending rigidity of the rock layers is also not considered. As such, a ubiquitous-joint material may miss-represent the yielding and deformation response of the rock mass if the response is not calibrated.

The Subiquitous model is a generalization of the Ubiquitous-Joint model which implements a bilinear Mohr–Coulomb failure envelope, together with strain softening/hardening behavior for both the matrix and joints. Within both the Ubiquitous and Subiquitous models, general failure is detected first based on the Mohr–Coulomb criteria for the matrix. Once the relevant plastic corrections are applied, new stresses are analyzed for failure on the plane of weakness and updated accordingly.

Verification of the response of the Ubiquitous-Joint model formulation is often provided by comparison with the single plane of weakness analytical solution developed

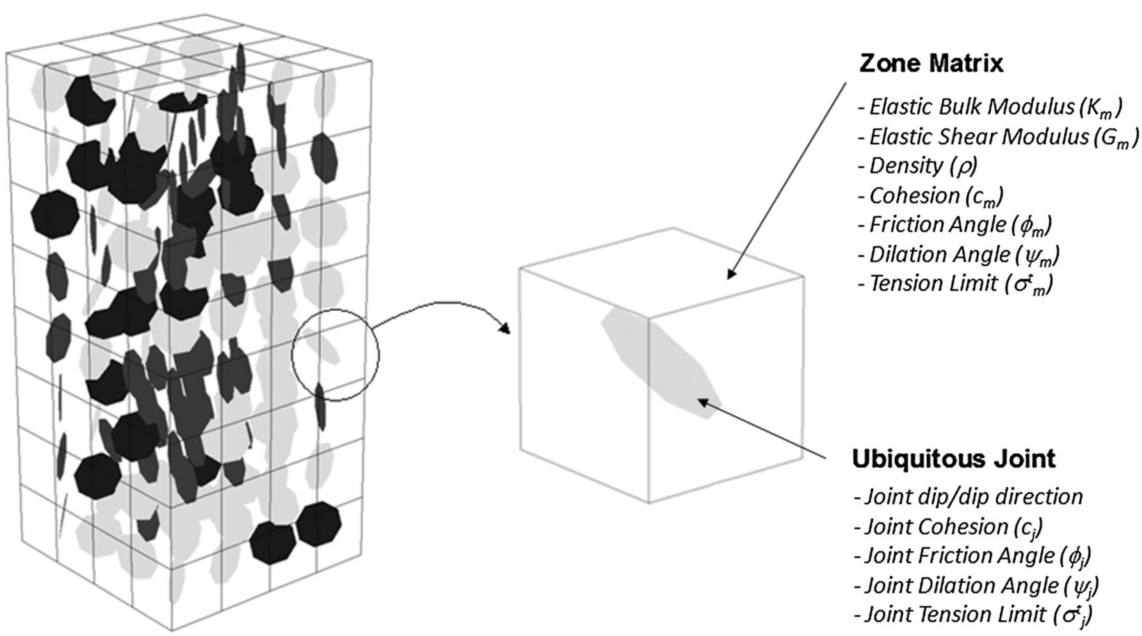

Fig. 2 Zone-based matrix and ubiquitous-joint properties (modified after Sainsbury et al. 2008)

by Jaeger (1960) and later described by Jaeger and Cook (1976). The solution states that slip on the discontinuity will occur, provided $1 - \tan\phi \tan\beta > 0$ if the following condition is satisfied:

$$\sigma_1 \geq \sigma_3 + \frac{2(c + \sigma_3 \operatorname{Tan}\phi)}{(1 - \operatorname{Tan}\phi \operatorname{Tan}\beta) \operatorname{Sin} 2\beta}$$

where c is the cohesive strength of the discontinuity, ϕ is the angle of friction and β is the angle of the discontinuity.

The simple solution only permits two independent failure modes (a) failure along the discontinuity and (b) failure through intact material. If $1 - \tan\phi \tan\beta \leq 0$, joint slip cannot occur, and the only alternative is failure of the rock matrix. Figure 3a illustrates the form of Jaeger's solution that results in a 'U-shaped' curve with shoulders. In this solution, failure along the plane of weakness is not possible for $\beta < \phi$ and $\beta = 90°$. Figure 3b compares results of the Ubiquitous-Joint model as implemented in *FLAC^{3D}* (Itasca 2011) to Jaeger's solution. A close match to the analytical compressive strength predictions is observed.

Hoek and Brown (1980) and Brady and Brown (2004) report that this analytical solution, while suitable for cases in which a single well-defined orientation of discontinuity is present in a rock specimen, is oversimplified and does not adequately describe the behavior of naturally occurring anisotropic rocks which exhibit continuous strength variation with increasing β angles. In reality, rocks usually exhibit a spread of orientation for the plane of weakness.

Laboratory triaxial testing on intact specimens reported by Donath (1972) and McLamore and Gray (1967) is presented in Fig. 4.

A review of these studies shows that strength does indeed vary continuously with the average weak plane orientation β. This observation of continuously variable strength with β has also been confirmed by many researchers who have studied the anisotropic behavior of rocks such as shales, slates, sandstone, gneisses and phyllites (Brown et al. 1977; Salcedo 1983; Singh et al. 1989) together with synthetic cement-based anisotropic specimens (Tien et al. 2006).

Al-Harthi (1998) provides a summary of the different idealized anisotropic curves reported throughout the literature. Ideally, a single plane of anisotropy, such as joint plane or bedding plane (Fig. 5, case I—solid line), produces a single U-shape curve with two shoulders which, accordingly, can be termed a shoulder-type anisotropy curve. A more realistic set of discontinuities such as lamination, foliation or cleavage, on the other hand, produces a U-type anisotropy curve with no shoulder (Fig. 5, case II—dashed line).

2.2 Cosserat Plasticity Models for Layered Rock

To overcome the limitations of the Ubiquitous-Joint model (where effects such as block interlocking, internal moments and rock layer bending stiffness are neglected), several researches have implemented user-defined Cosserat plasticity models into finite difference and finite element codes (Dawson and Cundall 1992, 1996; Mühlhaus 1993; Adhikary 2010; Riahi and Curran 2009). Cosserat continuum models contain additional rotational degrees of freedom not present in the Ubiquitous-Joint model and allow for moment stresses and a non-symmetric stress tensor. All the Cosserat models presented in the literature show accurate comparisons with discontinuum analyses of anisotropic rock masses. However, due to technical difficulties

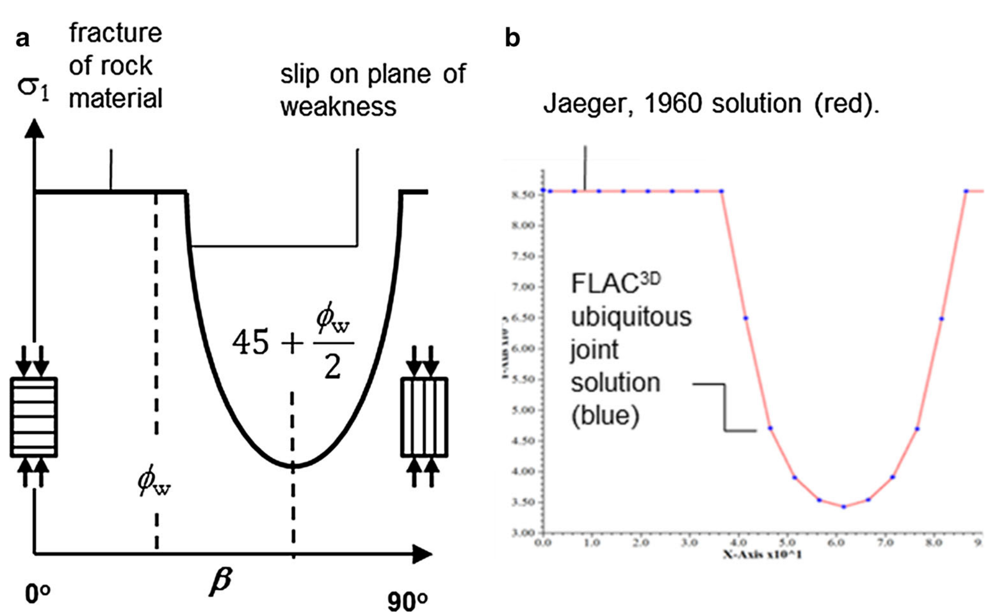

Fig. 3 **a** Jaeger's (1960) analytical solution for the effect of a single joint plane of weakness; **b** comparison of uniaxial compressive strength values—Ubiquitous-Joint model versus analytical solution

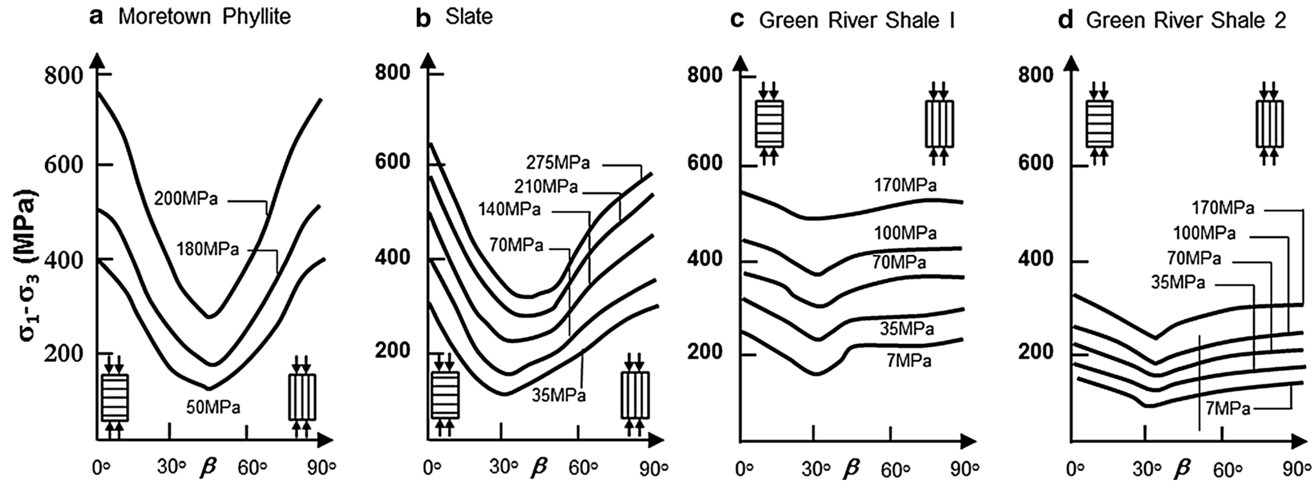

Fig. 4 Laboratory testing conducted on anisotropic intact laboratory samples (modified after Donath 1972; McLamore and Gray 1967)

Fig. 5 Typical strength anisotropy curves for samples with single, one set and two discontinuities [Al-Harthi (1998) modified after Hoek and Brown (1980)]

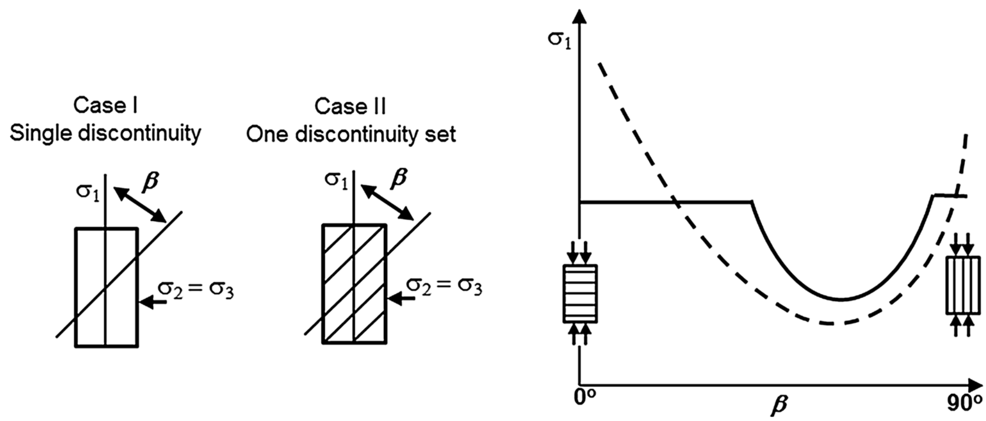

which include modification of grid points to be given additional rotational degrees of freedom, additional stress terms (couple stresses) and modification of the equations of motion, to date, a generalized Cosserat constitutive model has not been implemented in a commercial modeling code. As such, the Ubiquitous-Joint and Subiquitous models are still the most common constitutive models used for routine analysis of layered and anisotropic rock masses. The implementation and limitations of such models are explored herein.

3 Comparison Between Discontinuum and Ubiquitous-Joint Modeling Approaches in a Simulated Laboratory Environment

Naturally, discrete modeling techniques provide the most accurate description of discontinuous materials (Riahi and Curran 2009). Numerical experiments using discontinuum techniques provide significant insight and understanding into rock mechanics processes that are difficult to test in the laboratory (Fairhurst et al. 2006; Damjanac et al. 2007; Gao and Stead 2014).

Within this paper, a discontinuum model of a rock mass that is modeled at a size comparable to or above the representative elemental volume (REV) is considered to be the most accurate representation of the strength and deformation response of the sample. Implementations of the Ubiquitous-Joint model have been applied in its simplest form (two-dimensional, no strain softening) and most complex form (three-dimensional, strain softening) to represent the material response generated and compared to the discontinuum model results for comparison.

3.1 Response of Two-Dimensional Discontinuum and Ubiquitous-Joint Numerical Experiments

In order to investigate the strength and deformation behavior of an anisotropic, sedimentary rock mass, the two-dimensional distinct element code *UDEC* (Itasca 2011) has been used. Rock mass joint fabric has been explicitly modeled within a simulated large-scale (10 m high) unconfined compressive test. Separate analyses have been conducted simulating a joint spacing of 0.1 and 0.25 m, respectively. Randomly located orthogonal cross joints have been included to represent the discontinuous nature of a naturally occurring global response of a sedimentary rock mass. The model geometry is presented in Fig. 6. The properties used in the simulation are presented in Table 1.

A comparable Ubiquitous-Joint model has also been developed. The explicit block and joint properties outlined in Table 1 have been used directly as the matrix and ubiquitous-joint inputs to the Ubiquitous-Joint model that have also been run in UDEC. Both numerical experiments simulate a frictional interface between the specimen and loading platen. The anisotropic strength response of the discontinuum and Ubiquitous-Joint models is illustrated in Fig. 6.

As expected, the discontinuum models follow a continuously variable strength curve with increasing β angles. The Ubiquitous-Joint model does not show any effect of the weakness planes at β angles less than 27° which represents the friction strength of the joint. The post-peak softening response is also not well represented (Fig. 7b) at these angles in the Ubiquitous-Joint models. The effect of increased joint spacing (0.25 m) within the discontinuum model can be observed to increase strength at β angles less than 45°—bringing the results closer to the Ubiquitous-Joint model. The shoulders on the Ubiquitous-Joint U-curve clearly shows a limitation of this approach when the loading direction is sub-perpendicular (β angles less than 45°) to the predominant joint orientation.

The individual stiffness and stress–strain responses of the discontinuum and Ubiquitous-Joint models for varying β angles are presented in Fig. 7. Clearly, when the rock block elastic parameters are used directly in the Ubiquitous-Joint model, the resulting deformation modulus is significantly higher than the discontinuum response (Fig. 7a). This is most noticeable at β angles of 60° when only the joints are being mobilized. This variation in stiffness response between the Ubiquitous-Joint and discontinuum models is a direct result of the ubiquitous-joints not having a stiffness associated with them. Care should be taken when using this approach for engineering design, since the stiffness response of the system will be over-represented most notably at β angles 50°–60°.

Based on the bedding thickness simulated in the UDEC models that ranged from 0.1 to 0.25 m, it may be appropriate to apply the Ubiquitous-Joint model (as demonstrated) with the explicit block and joint properties used directly as the matrix and ubiquitous-joint inputs when bedding spaces greater than those simulated are measured and cross-jointing is not observed in the rock mass specimen. This is almost never the case. Scale effects, in relation to the size of the excavation and the rock mass bedding thickness, are likely to play a role in the response here. It is therefore recommended that explicit block and joint properties never be used as direct inputs for the matrix and ubiquitous-joint properties. In order to use a Ubiquitous-Joint model to produce meaningful results, calibration of the matrix and ubiquitous-joint parameters is required to match the discontinuum response. This calibration is further explored for a complex three-dimensional sample below.

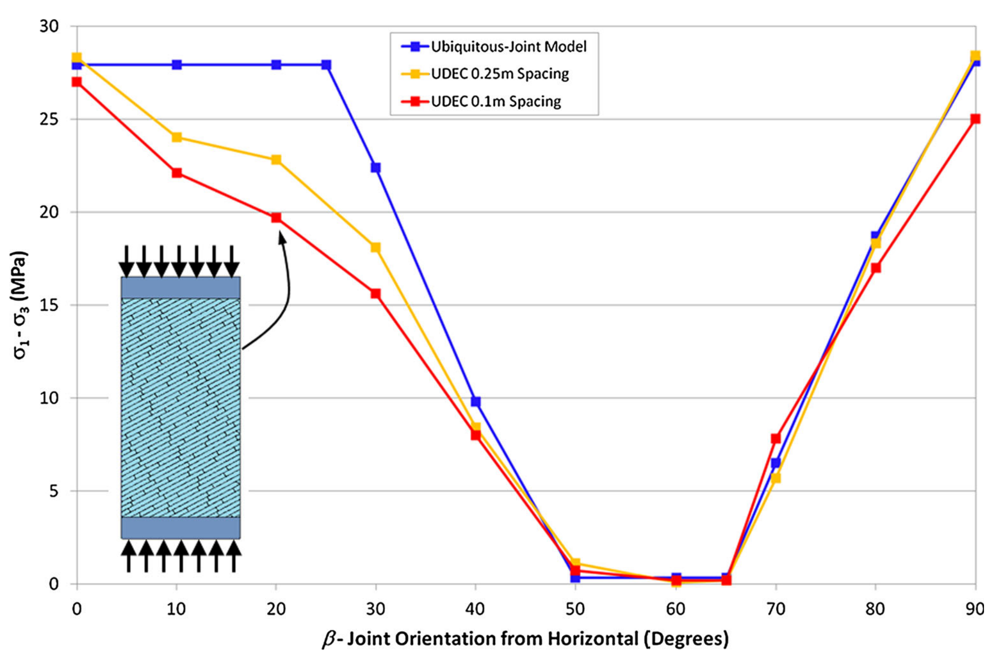

Fig. 6 Anisotropic strength of discontinuum and Ubiquitous-Joint models

Table 1 Rock and joint mechanical properties

Block properties					Joint properties				
E (GPa)	ν	c (MPa)	ϕ (°)	σ_t (MPa)	kn (GPa/m)	ks (GPa/m)	c (MPa)	ϕ (°)	σ_t (MPa)
40	0.2	6.5	42	4.9	100	10	0.1	27	0.0

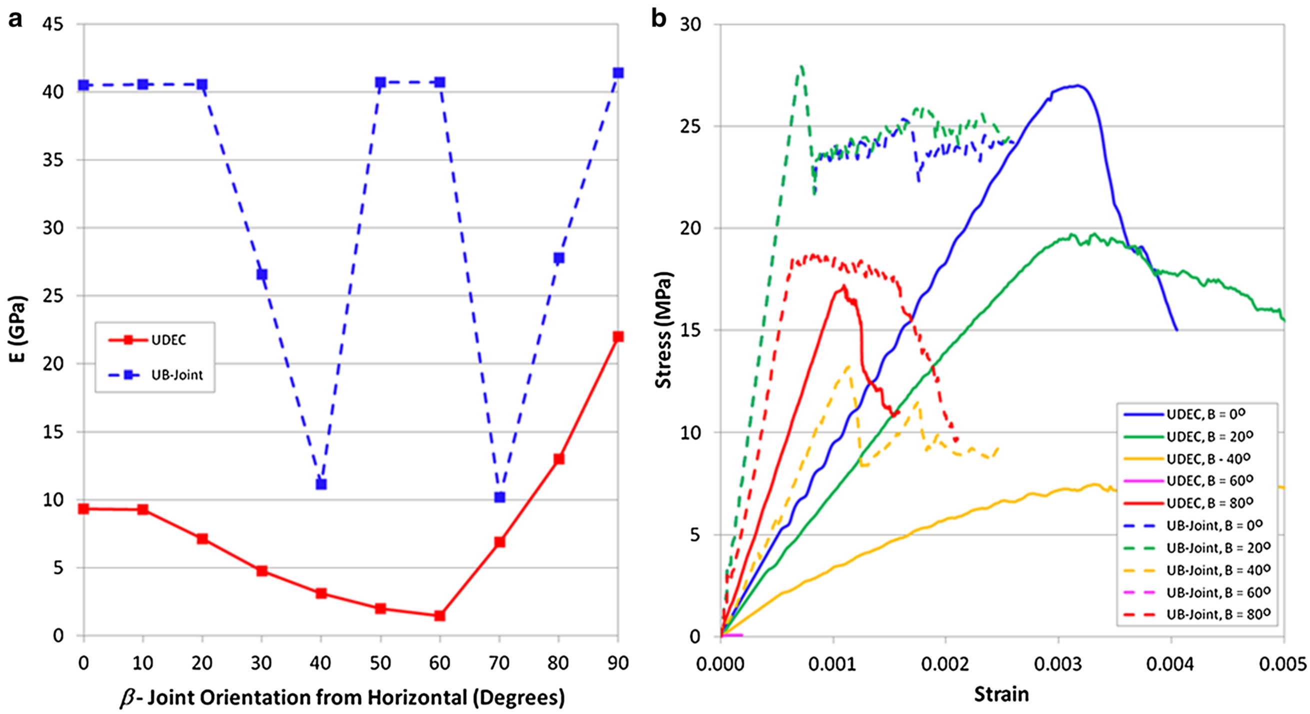

Fig. 7 **a** Deformation modulus of discontinuum and Ubiquitous-Joint models, **b** stress–strain response of discontinuum and Ubiquitous-Joint models

3.2 Calibration of a Two-Dimensional Subiquitous Material

The Subiquitous model offers greater flexibility associated with modifying matrix and ubiquitous-joint parameters than the Ubiquitous-Joint model. Through the implementation of a bilinear softening relation, better representation of the strength and deformation behavior of layered and anisotropic rock masses can be achieved with a Subiquitous model in comparison with the Ubiquitous-Joint model. A systematic procedure has previously been developed (Sainsbury et al. 2008, 2016a, b; Sainsbury 2012; Sainsbury and Sainsbury 2013) to calibrate Subiquitous model properties to the response of an equivalent discontinuum numerical experiment.

The methodology for selecting and validating material responses has previously been applied and validated at the Palabora Mine in South Africa (Sainsbury et al. 2008; Sainsbury et al. 2016a, b) through a large-scale implementation. An example of the complex damage behavior that can be represented within a subiquitous sample with three joint sets is presented in Fig. 8. It can be seen that during the early stages of sample loading ubiquitous-joint tensile and shear failure are the dominant yielding modes within the sample. As the sample reaches the peak strength of the rock mass, matrix shear commences resulting in degradation of the intact rock blocks and collapse of the sample.

Assumptions used in the subiquitous calibration procedure include:

(a) The results of the discontinuum analyses accurately quantify rock mass anisotropic behavior.
(b) The measured or observed bedding plane cohesion and friction angle must be used to describe the peak ubiquitous-joint strength. This ensures the synthetic sample provides a close match to the shear strength of the rock mass under planar sliding conditions. Joint cohesion is softened to zero at the same softening rate as the matrix cohesion.
(c) The matrix strength and deformation response must be calibrated to compensate for the length scale and lack of stiffness parameters in the ubiquitous-joint formulation. This is completed through the inclusion

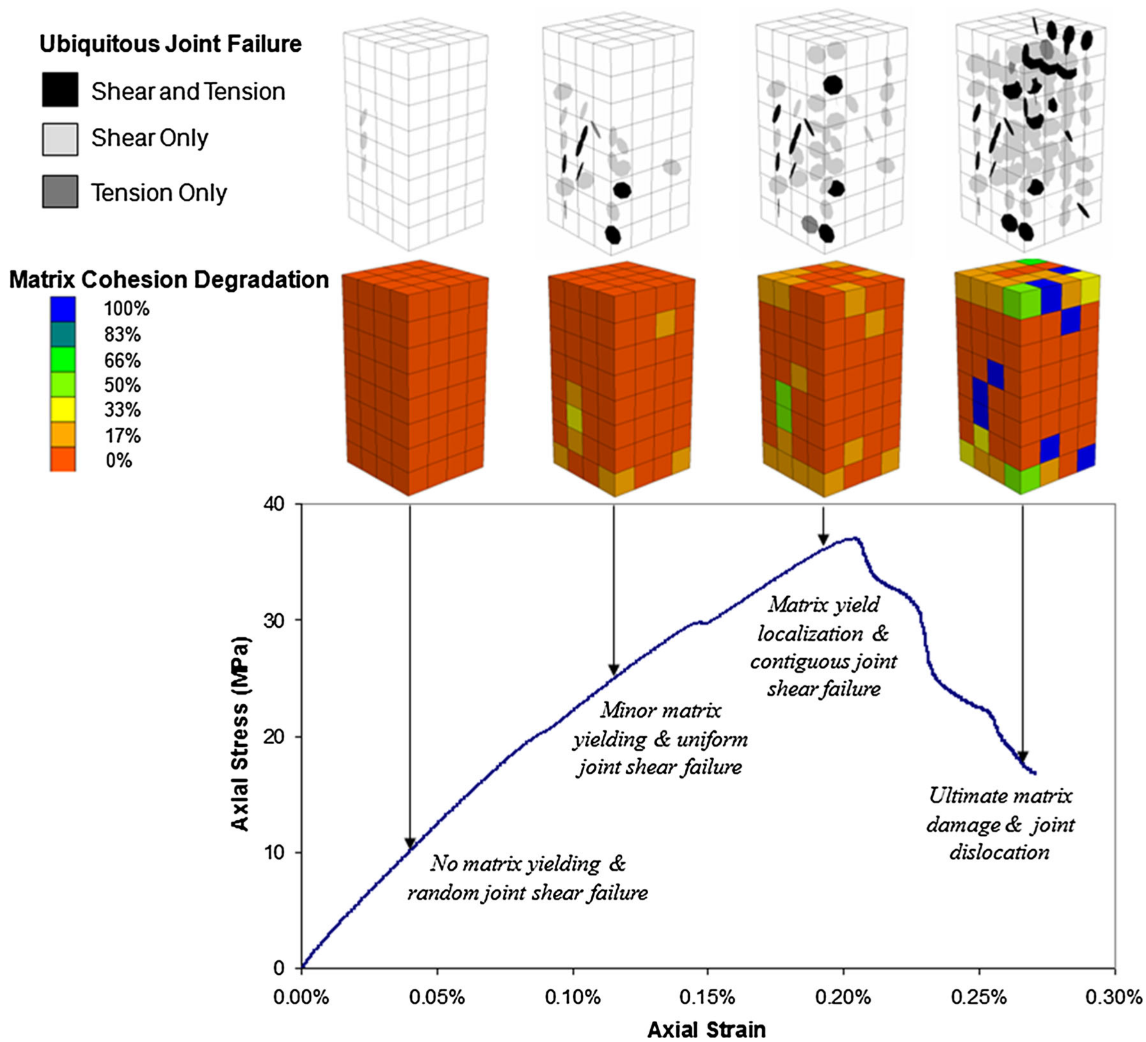

Fig. 8 Stages of damage within a calibrated Subiquitous model including matrix cohesion degradation and ubiquitous-joint failure

of an orthogonal ubiquitous-joint set and matching the post-peak response of the discontinuum analyses stress–strain curve through modification of the matrix strength and softening rate.

1. Orthogonal ubiquitous-joint set
Through an initial Subiquitous model calibration process, the authors discovered that in order to better represent a naturally occurring anisotropic rock mass strength and deformation response, some ubiquitous-joints within the rock mass that are randomly seeded should be re-orientated orthogonal to the dominant joint/bedding fabric. The inclusion of orthogonal ubiquitous-joints promotes continuously variable strength with increasing average β angles within the sample (i.e., resolves the artificial shoulders in the strength U-curves). Furthermore, heterogeneity is introduced into the ubiquitous-joint system that limits artificial yielding/banding (presented in Fig. 11) while still capturing and maintaining the global anisotropic response. The actual percentage of re-oriented orthogonal joints should be varied to calibrate the desired stiffness results. The authors have achieved acceptable results with values of re-oriented joints between 5 and 20% (Sainsbury et al. 2016a, b).

2. Matrix strength and softening
The peak strength of a Subiquitous specimen at β angles of 0° and 90° is dependent on the matrix cohesion, friction and tensile strength. These strength parameters are selected based on a calibration of the matrix material response to the discontinuum strength at a β angle = 0°. In the interest of simplicity, it is assumed that cohesion and tension soften to zero with accumulated plastic strain. The rate at which softening occurs is calibrated to the post-peak response of the equivalent discontinuum experiment. It is important to note that when introducing softening into the constitutive model, it

is important to ensure that the zone size used in the numerical experiment is the same used in the subsequent large-scale simulations.

Throughout the calibration process, both the strength and stiffness parameters are honored along with the failure/damage evolution within the samples. Failure mechanisms within the discontinuum and Subiquitous models are compared and categorized as tensile spitting along discontinuities (loading sub-parallel to bedding, $\beta \sim 90°$), sliding failure along discontinues ($\beta \sim 60°$) and sliding and tensile failures across discontinuities (characterized by matrix and ubiquitous-joint failure). Confirmation of the correct failure mechanism within the subiquitous sample is completed through the monitoring of progressive matrix degradation, joint slip and joint dislocation during failure. Generalized guidelines for the calibration of a Subiquitous model to a synthetic sample and/or field and laboratory measurements are provided in Table 2. The development and validation of these values are documented in Sainsbury (2012).

The two-dimensional numerical experiments outlined in Sect. 3.1 have been recreated with a calibrated Subiquitous model. Table 3 provides a summary of the calibrated subiquitous material properties used to represent the discontinuum material with 0.1 m joint spacing. An orthogonal joint set that represents up to 10% of the ubiquitous-joint zones has been represented in the model.

The anisotropic U-curves of the discontinuum and subiquitous responses are presented in Fig. 9. The original Ubiquitous-Joint model results are also provided for comparison.

The calibrated Subiquitous model provides a close match to the continuously variable strength response developed in the discontinuum analysis. Individual stiffness and stress–strain responses for the calibrated subiquitous material at selected β angles are presented in Fig. 10. A close match to the deformation modulus and post-peak response of the discontinuum model is also achieved.

4 Analysis of the Performance of a Two-Dimensional Circular Tunnel with Discontinuum, Ubiquitous-Joint and Subiquitous Models

To demonstrate the performance of the calibrated Subiquitous model developed in Sect. 3.2 in a more complex stress field, the calibrated response has been exercised in a simple two-dimensional tunnel model that has been developed in an isotropic stress field, with zero gravity. For comparison of the model results, a discontinuum model with 0.1 m spacing and equivalent Ubiquitous-Joint model have been simulated. The tunnel has a diameter of 4 m. Figure 11 compares the yield state, displacement and major principal stress within each model at the completion of the tunnel excavation.

The discontinuum model shows minor yielding of the intact blocks in the sidewalls of the tunnel with joint slip extending approximately 1.5 m from the roof and floor of the tunnel—perpendicular to the major joint set (Fig. 11a). The maximum displacement in roof and floor of the discontinuum model is approximately 8 mm (Fig. 11b).

The Ubiquitous-Joint model (which uses the explicit block and joint properties directly for the matrix and ubiquitous-joint input parameters) shows no matrix failure but significant ubiquitous-joint tensile failure extending in bands

Table 2 Generalized input parameters for the calibration of a Subiquitous model

Matrix	
Deformation modulus	10% of intact modulus measured in laboratory
Poisson ratio	0.25 based on Hoek et al. (1995)
Cohesion	50% intact value estimated from HB strength criteria with GSI 100
Tension	10% matrix cohesion
Friction (°)	42–45° based on fully bulked and intact value
$\epsilon_{\rm crit}^{\rm ps}$	−0.0142GSI + 1.3967 based on Sainsbury (2012) and scaled for zone size
Joint	
Cohesion	Direct input of observed values
Friction	Direct input of observed values
Tension	0
$\epsilon_{\rm crit}^{\rm ps}$	1–100% matrix value

Table 3 Calibrated subiquitous mechanical properties

Matrix properties						Ubiquitous-joint properties			
E (GPa)	v	c (MPa)	ϕ (°)	$\sigma_{\rm t}$ (MPa)	$\epsilon_{\rm crit}^{\rm ps}$ (%)	c (MPa)	ϕ (°)	$\sigma_{\rm t}$ (MPa)	$\epsilon_{\rm crit}^{\rm ps}$ (%)
10	0.2	6.4	45	0.64	0.016	0.1	27	0	0.016

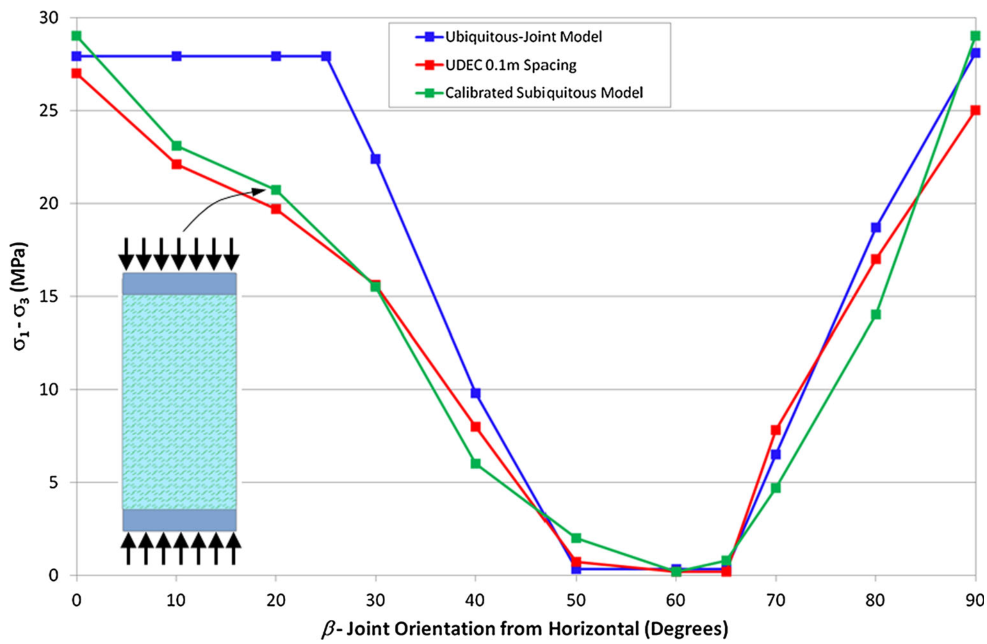

Fig. 9 Anisotropic strength of discontinuum and calibrated Subiquitous model

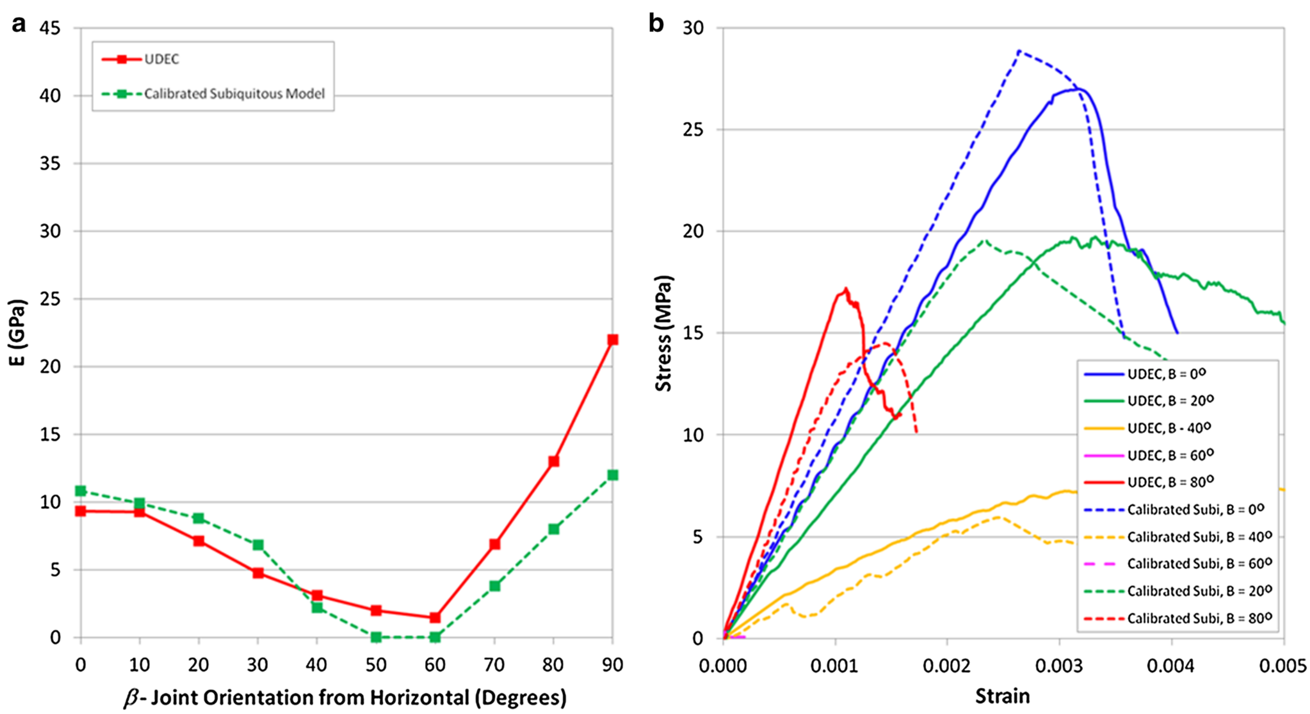

Fig. 10 **a** Deformation modulus of discontinuum and calibrated Subiquitous models, **b** stress–strain response of discontinuum and calibrated Subiquitous models

approximately one tunnel diameter (4 m) from the roof and floor (Fig. 11d). The ubiquitous-joint tensile failure causes significant stress redistribution around the yielded zones in roof and floor of the model (Fig. 11f). The maximum displacement in the model is significantly lower than the discontinuum model (Fig. 11e). The artificial ubiquitous-joint tensile failure mechanism is caused by the inability of the ubiquitous-joint formulation to account for the bending stiffness of the individual layers of rock. Figure 12 illustrates the deformed blocks of the discontinuum model that have been magnified 100 times. Bending of the rock layers can be clearly observed in the roof and floor of the tunnel. The interlocking of the rock layers with finite joint spacing gives rise to moments that resist the imposed distortions.

The results of the calibrated Subiquitous model show a response that is closer to the discontinuum model. Minor

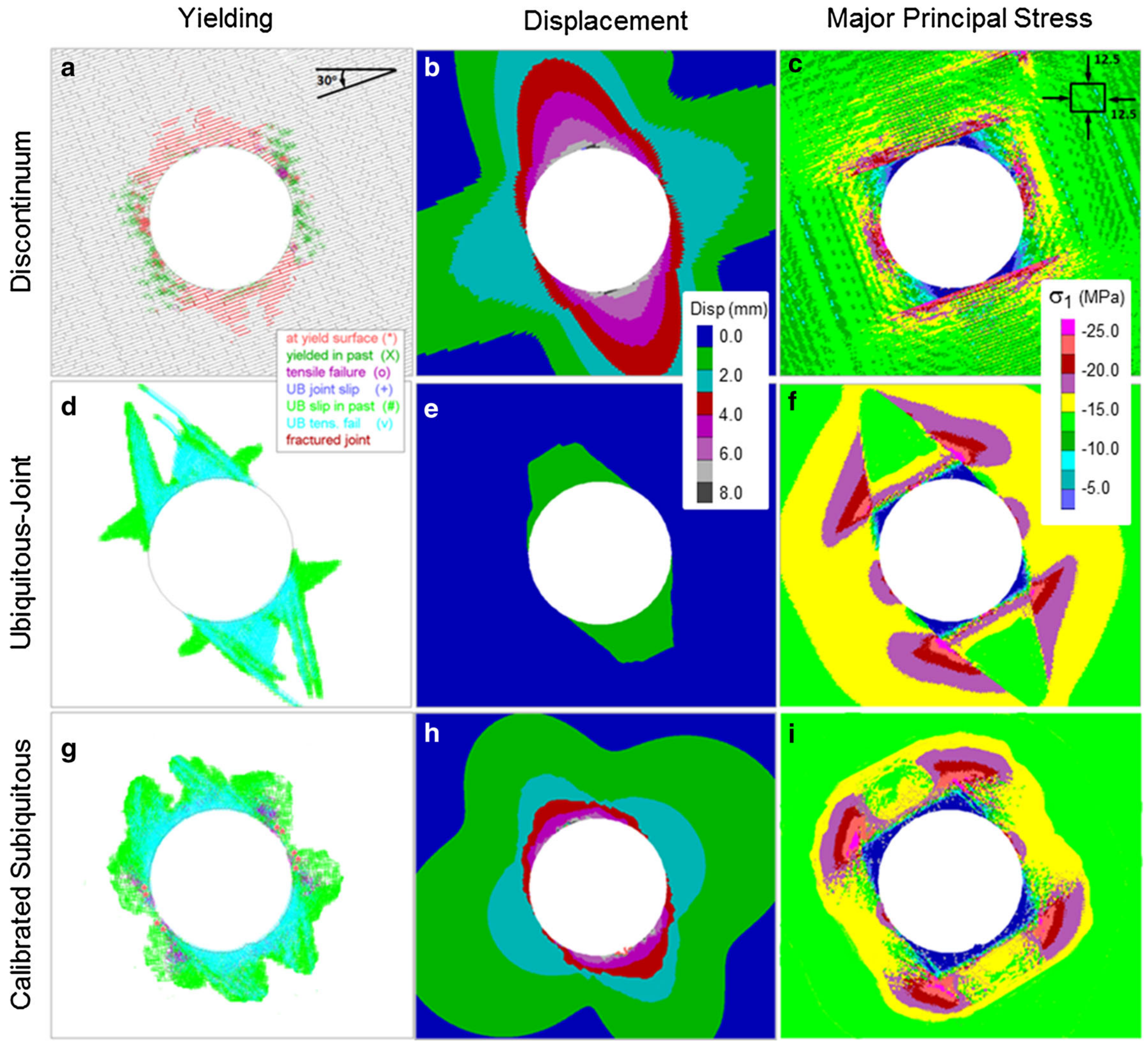

Fig. 11 Yielding, displacement and major principal stress around 4-m-diameter tunnel

yielding of the matrix is predicted in the sidewalls of the tunnel with ubiquitous-joint slip and tensile failure extending approximately 2.0 m from the roof and floor of the tunnel (Fig. 11g). Re-orientation of 20% of the ubiquitous-joints orthogonal to the average joint orientation assists in introducing some bending resistance within the system. However, this does not resolve the effect of block interlocking. The reduced ubiquitous-joint yielding provides a more representative stress redistribution around the tunnel (Fig. 11i), and the displacement profile is more consistent with the discontinuum model.

5 Analysis of a Two-Dimensional Anisotropic Open Pit Slope Failure

Several of the rock mass units encountered in the Pilbara region of Western Australia exhibit clear rock mass strength and deformation anisotropy, generally due to the presence of relatively weak bedding planes and shale bands. Past slope failures in the Pilbara iron ore operations have often been controlled by the presence of these discontinuities. Figure 13 illustrates a banded iron formation (BIF) rock mass with high intact strength and relatively weak bedding plane shear strength.

The basic rock mass parameters used to describe a generic BIF material are presented in Table 4. These material properties have been developed based on extensive laboratory testing and *in situ* characterization across a number of sites.

5.1 Discontinuum and Subiquitous Large-Scale Loading Simulation of BIF Material

In order to provide greater understanding of the anisotropic rock mass strength and deformation behavior of the generic BIF material, a series of large-scale (10 m) simulated compression tests have been conducted within the three-

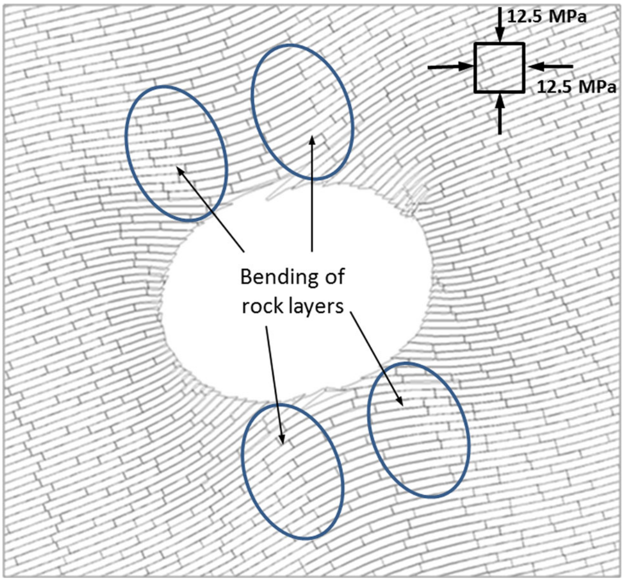

Fig. 12 Deformed blocks within discontinuum model, magnified 100 times

dimensional distinct element code *3DEC* (Itasca 2007). Bedding plane spacing of ~0.2 m was assigned together with two orthogonal, non-persistent joint sets. The spacing and persistence of the joint sets was assigned to ensure the average block volume within the sample is ~0.3 m^3, which is consistent with an observed average GSI of 60 (Cai et al. 2007).

To account for the significant impact that micro-flaws (pores, open cracks, veins) and weathering/alteration can have on the strength scale effect, the simulated rock block strength was 80% of the σ_{ci} for the intact BIF. This value is based on an empirical scale effect relation developed by Hoek and Brown (1980) and extended by Yoshinaka et al. (2008). Figure 14 illustrates the UCS response of the generic BIF material at a β angle of 0°.

In order to develop robust calibrated subiquitous material properties, the same procedure as described in Sect. 3.2 was conducted in *FLAC^{3D}*. Figure 15 illustrates a comparison of the anisotropic strength achieved in both the three-dimensional discontinuum and Subiquitous models. At each simulated β angle, both the peak strength and failure mode within the discontinuum and subiquitous samples were honored.

5.2 Discontinuum and Subiquitous Simulation of Anisotropic Pit Slope Failure

The occurrence of slope failure mechanisms controlled by the orientation of weak bedding planes at BHP Billiton's Mt Whaleback Mine was first reported by Kale and Trudinger (1975). Figure 16 illustrates a schematic design section used to assess slope stability within a BIF material. The overall bedding is favorably oriented for stability with exceptions that occur in the synclinal keel areas designated as failure surfaces A, B and C.

In order to demonstrate the behavior of the calibrated Subiquitous model when applied to a slope stability problem, a *FLAC^{3D}* model was developed to simulate the basic geometry and failure mechanisms reported by Kale and Trudinger (1975). Figure 17 illustrates the 1-m thick *FLAC^{3D}* model where the ubiquitous-joints have been

Fig. 13 Generic BIF material

Table 4 Basic parameters used to describe BIF material

Rock mass properties			Joint properties			
GSI	σ_{ci} (MPa)	m_i	Bedding spacing (m)	c (kPa)	ϕ (°)	σ_t (MPa)
60	150	10	0.2	44	33	0.0

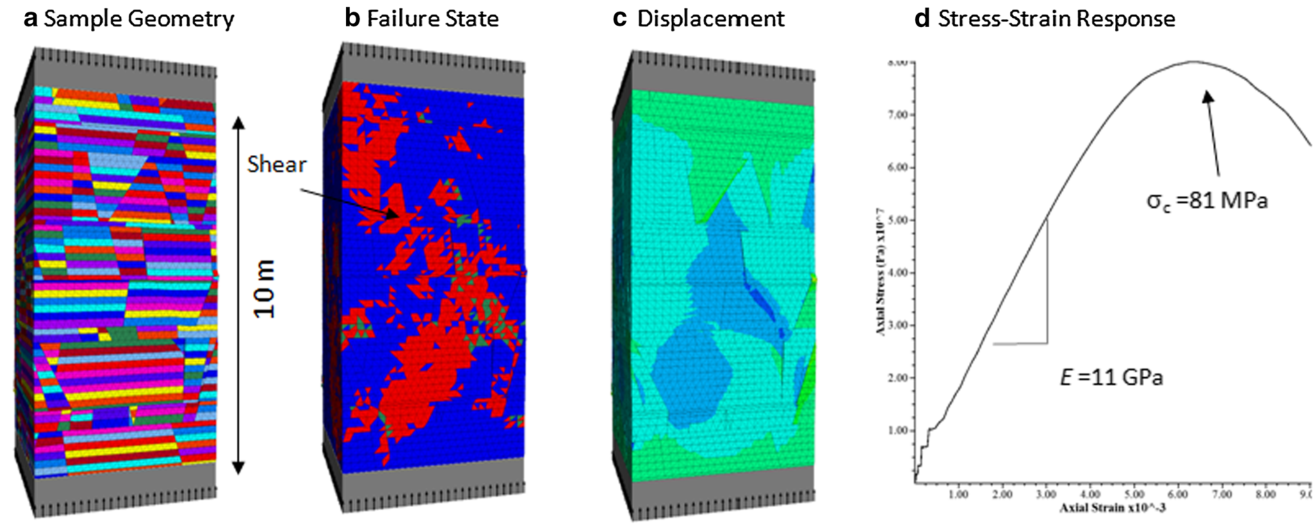

Fig. 14 *3DEC* model of simulated BIF material, $\beta = 0$, $\sigma_3 = 0$ MPa

Fig. 15 Anisotropic strength of three-dimensional discontinuum and calibrated Subiquitous model

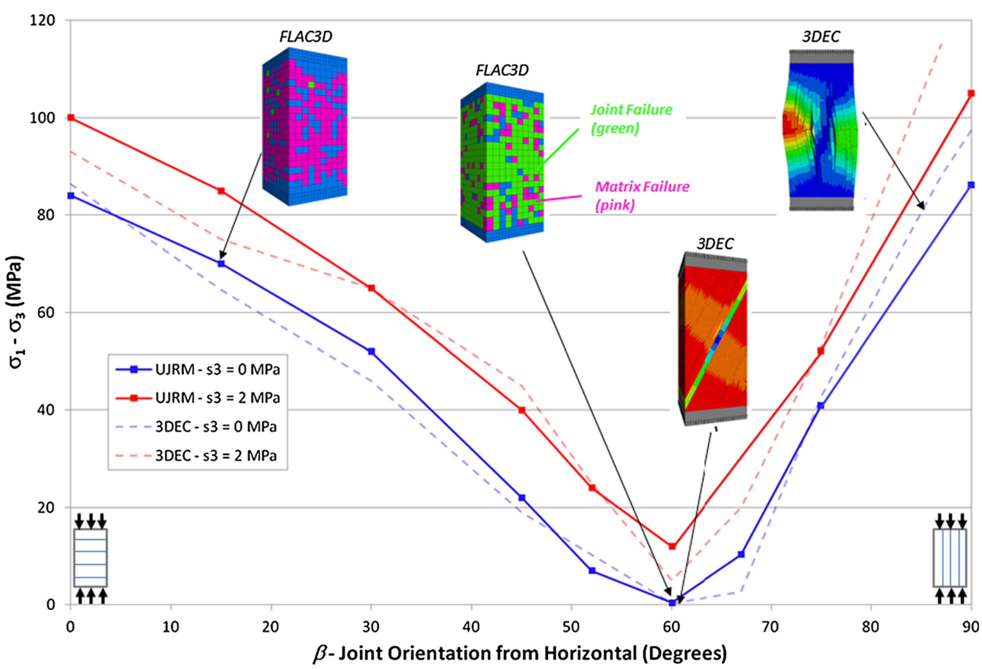

assigned based on a number of conceptual bedding traces. To provide confidence in the Subiquitous modeling results, a two-dimensional *UDEC* model was also constructed. The bedding and cross joints have been simulated explicitly within this model. The simulation results are presented in Fig. 17 for each of the models.

The $FLAC^{3D}$ Subiquitous model predicts failure of the synclinal keel areas within the upper portion of the slope providing a close match to the response of the discontinuum model. This demonstrates that emergent failure mechanisms due to changing stress conditions within a subiquitous model can be simulated with confidence. Failure mechanism associated with block toppling and wedge failure using this approach has previously been explored in Sainsbury and Sainsbury and Sainsbury (2013) and Sainsbury et al. (2016a).

6 Analysis of Three-Dimensional Anisotropic Deformation in an Underground Excavation

6.1 The Ballarat Gold Project

The Ballarat Gold Project is owned and operated by Castlemaine Goldfields Limited and is located in the city of Ballarat, Victoria, Australia. Cut and fill and stoping mining methods are used to extract gold from mining compartments that range from depths of 450 m to 695 m. Historical stress measurements conducted at the site suggest that the principal stress magnitudes are 2:1 (horizontal to vertical) and are aligned with the dominant bedding orientation that strikes approximately north–south and has a sub-vertical dip. The inter-bedded sandstone, siltstone, shale and quartz rock mass domains exhibit anisotropic

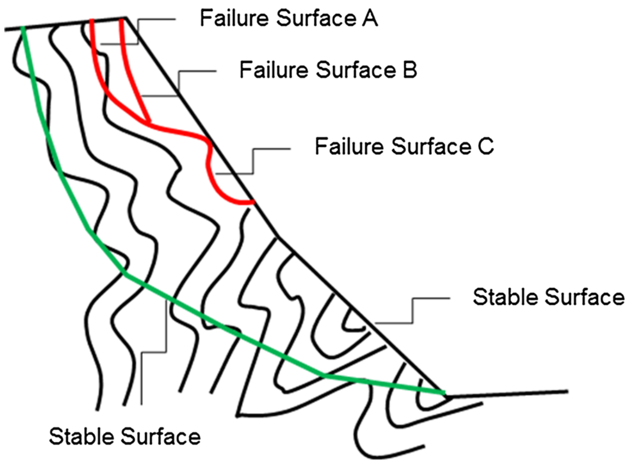

Fig. 16 Failure surfaces within a typical design section (after Kale and Trudinger 1975)

deformation responses during excavation development. Standard excavation profile is arched: 5.0 m width by 5.3 m height.

The Woah Hawp decline was developed for exploratory access at a depth of approximately 650 m. The decline was developed parallel to the main bedding fabric. Immediately after excavation, anisotropic deformation mechanisms were observed and rehabilitation due to excessive sidewall convergence was required. The typical performance of excavations at the Ballarat Gold Project driven parallel and perpendicular to the bedding is presented in Fig. 18.

Good ground conditions are usually encountered perpendicular to the bedding with only mesh and bolts required. Little rehabilitation is required in these drives. Excavations parallel to the bedding require significant rehabilitation due to over-break (that occurs during scaling and the installation of ground support). Shotcrete and additional bolting is usually required over the mesh.

Typical rock mass properties for the inter-bedded sandstone, siltstone and shale rock mass in the vicinity of the Woah Hawp decline around the 650 Level are presented in Table 5. These material properties have been developed based on laboratory testing and *in situ* characterization.

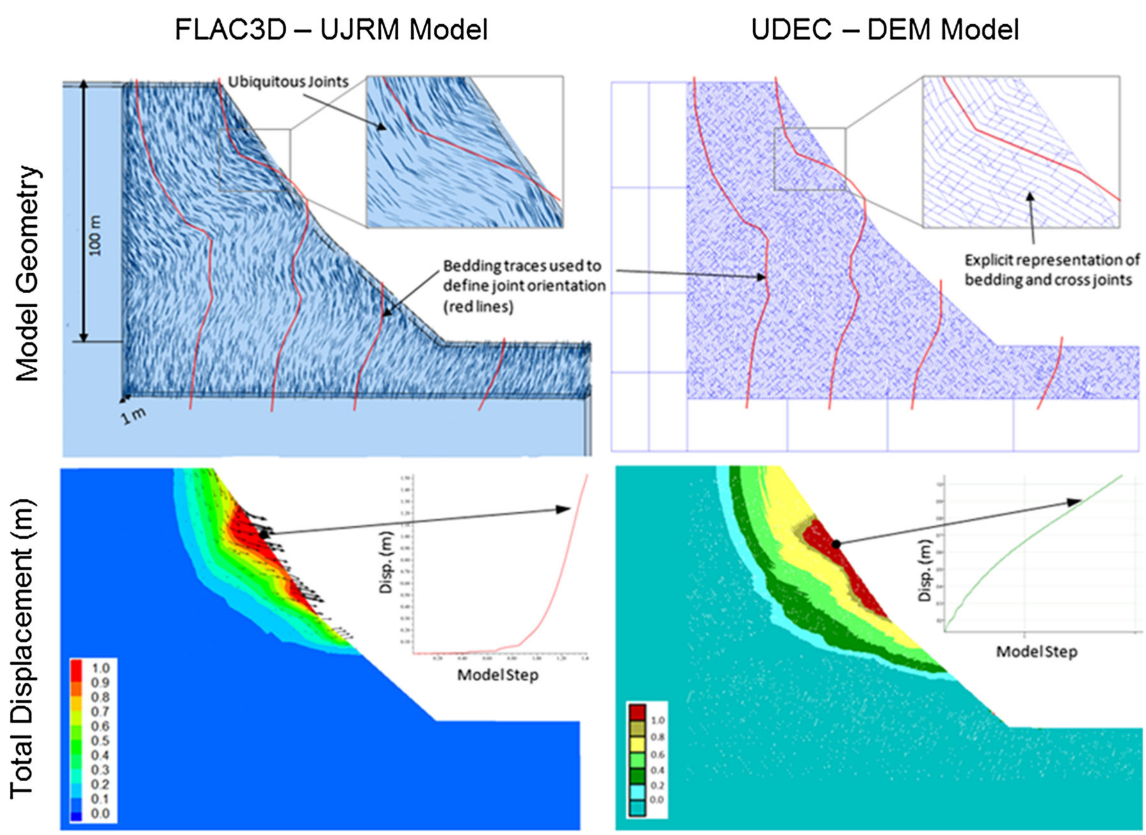

Fig. 17 Comparison of Subiquitous and discontinuum slope response

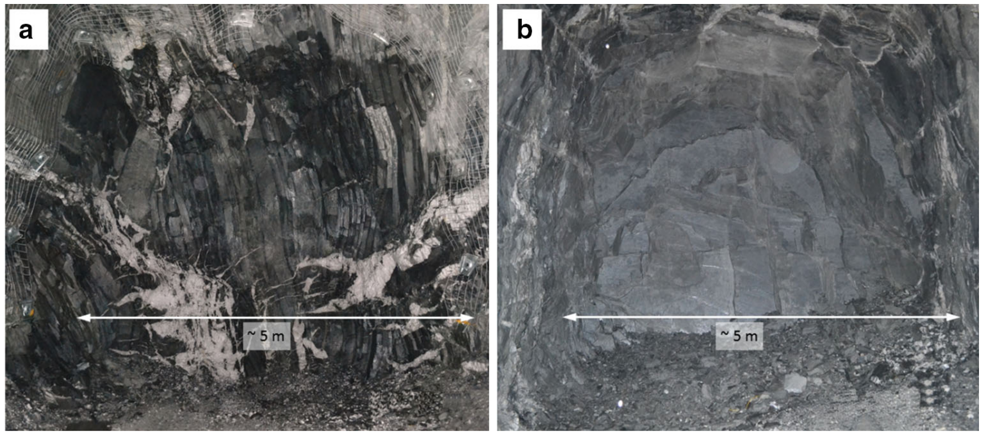

Fig. 18 Observed anisotropic rock mass **a** parallel and **b** perpendicular to excavation

Table 5 Basic parameters used to describe inter-bedded rock mass

Rock mass properties			Joint properties			
GSI	σ_{ci} (MPa)	m_i	Bedding spacing (m)	c (kPa)	ϕ (°)	σ_t (MPa)
48	50	6	0.05–0.2	44	18	0.0

6.2 Discontinuum and Subiquitous Large-Scale Loading Simulation of the Inter-bedded Rock Mass

A series of large-scale (10 m) simulated compression tests have been conducted within the three-dimensional distinct element code *3DEC* (Itasca 2012). A bedding plane spacing of approximately 0.05–0.2 m was assigned to the inter-bedded sandstone, siltstone, shale and quartz rock mass, together with two orthogonal, non-persistent joint sets. The spacing and persistence of the joint sets was assigned to ensure the average block volume within the sample was approximately 0.01 m^3 (after Cai et al. 2007) that is consistent with an observed GSI of 35. The rock block strength in *3DEC* was simulated at 80% of the σ_{ci} for the intact material based on drive-scale observations. The *3DEC* model used to simulate a REV of the rock mass is illustrated in Fig. 19.

A summary of the properties used to characterize the rock mass are presented in Table 6. They are based on the laboratory testing and *in situ* characterization data provided in Table 6 and in situ geotechnical observations.

Figure 20 illustrates the UCS stress–strain response of the simulated material with β angles of 15° and 75°.

In both of these samples, the strength and deformation behavior observed in the Woah Hawp decline are honored. For example, loading sub-perpendicular to bedding ($\beta = 15°$) results in a stiff, brittle response as shear failure causes failure of the intact rock blocks. Sliding along the discrete bedding planes at a β angle of 75° results in a weak, ductile loading response.

In order to derive subiquitous material properties, the same calibration procedure described in Sect. 3.2 was conducted in *FLAC^{3D}*. Figure 21 illustrates a comparison of the anisotropic strength achieved in both the three-dimensional discontinuum and subiquitous laboratory experiments.

Table 7 provides the calibrated Subiquitous material properties used to represent the discontinuum material.

A summary of the measured/estimated and calibrated subiquitous properties for the Ballarat Gold Project is provided in Table 8. These values are consistent for each of the calibrated subiquitous rock mass materials presented herein.

7 Tunnel-Scale Discontinuum and Subiquitous Simulation of the Inter-Bedded Rock Mass

The tunnel-scale response of the inter-bedded sandstone–siltstone–shale discontinuum and calibrated subiquitous material has been investigated through the development of a localized tunnel-scale model. Each of them is illustrated in Fig. 22.

A comparison of the simulated excavation responses using each of the techniques is provided in Fig. 23. The explicit (3DEC) model is considered to be the most rigorous representation of this rock mass. However, the calibrated Subiquitous model (developed in FLAC^{3D}) provides a close match to the anisotropic deformation, stress redistribution and yielding response observed in the discontinuum model. This provides confidence in being able to apply the more efficient calibrated subiquitous modeling technique to larger, regional modeling applications as discussed in Section 5.4.

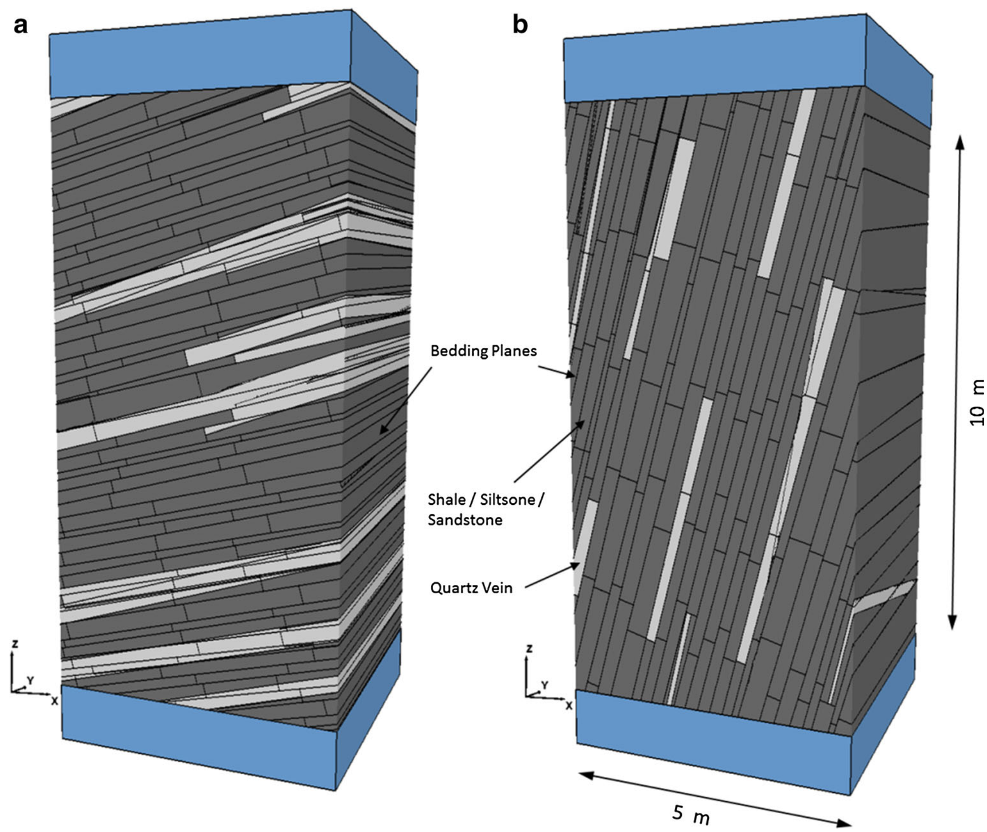

Fig. 19 3DEC model geometry—REV of inter-bedded sandstone, siltstone and shale rock at the Ballarat Gold Project

Table 6 Rock and joint mechanical properties

Block properties					Joint properties				
E (GPa)	*v*	*c* (MPa)	ϕ (°)	σ_t (MPa)	kn (PGa/m)	ks (GPa/m)	*c* (MPa)	ϕ (°)	σ_t (MPa)
85	0.25	30.5	31	3.5	100	10	0.02	18	0.0

7.1 Subiquitous Simulation of the Inter-Bedded Rock Mass Within the Woah Hawp Decline

As discussed, it is currently not practical to explicitly simulate the joint fabric of an entire rock mass in a discontinuum model for the analyses of large-scale excavations. In order to simulate the anisotropic rock mass response of an intersection within the Woah Hawp decline at the Ballarat Gold Project, a *FLAC*^{3D} model was constructed which includes approximately 110 m length of the decline, as illustrated in Fig. 24.

The calibrated subiquitous material properties derived for the inter-bedded sandstone–siltstone–shale presented in Table 6 were assigned. Progressive excavation of the Woah Hawp decline was simulated in 2.4 m advances within the model that is consistent with the development advance during excavation. The anisotropic deformation response of the model at the completion of development is presented in Fig. 25 along with in situ observations.

General observations from the model show that the greatest deformation is simulated in the walls of the excavation that strike north–south (parallel to the bedding—Fig. 26a). This is consistent with underground observations presented in Fig. 26c. Minor damage is simulated (Fig. 26a) and observed (Fig. 26b) to occur at the decline–stockpile intersection. Damage within the stockpile that strikes perpendicular to the bedding is simulated (Fig. 26a) and observed (Fig. 26d) to be minimal. A section through the model at locations A–A and B–B are provided in Fig. 27 below.

Section A–A presents the displacement and yielding results in the decline sidewalls that strike parallel to the bedding partings. The magnitude of displacement within the Subiquitous model is consistent with the convergence observations that are presented in Fig. 27. Approximately 120 mm of displacement is simulated parallel to the bedding within the sidewalls. Less than 20 mm of displacement is simulated (and observed) within the stockpile (Section B–B). The dominant failure mode within the decline is shear along bedding partings with joint separation occurring up to 5 m behind the face. Within the stockpile, few bedding joints are mobilized due to their

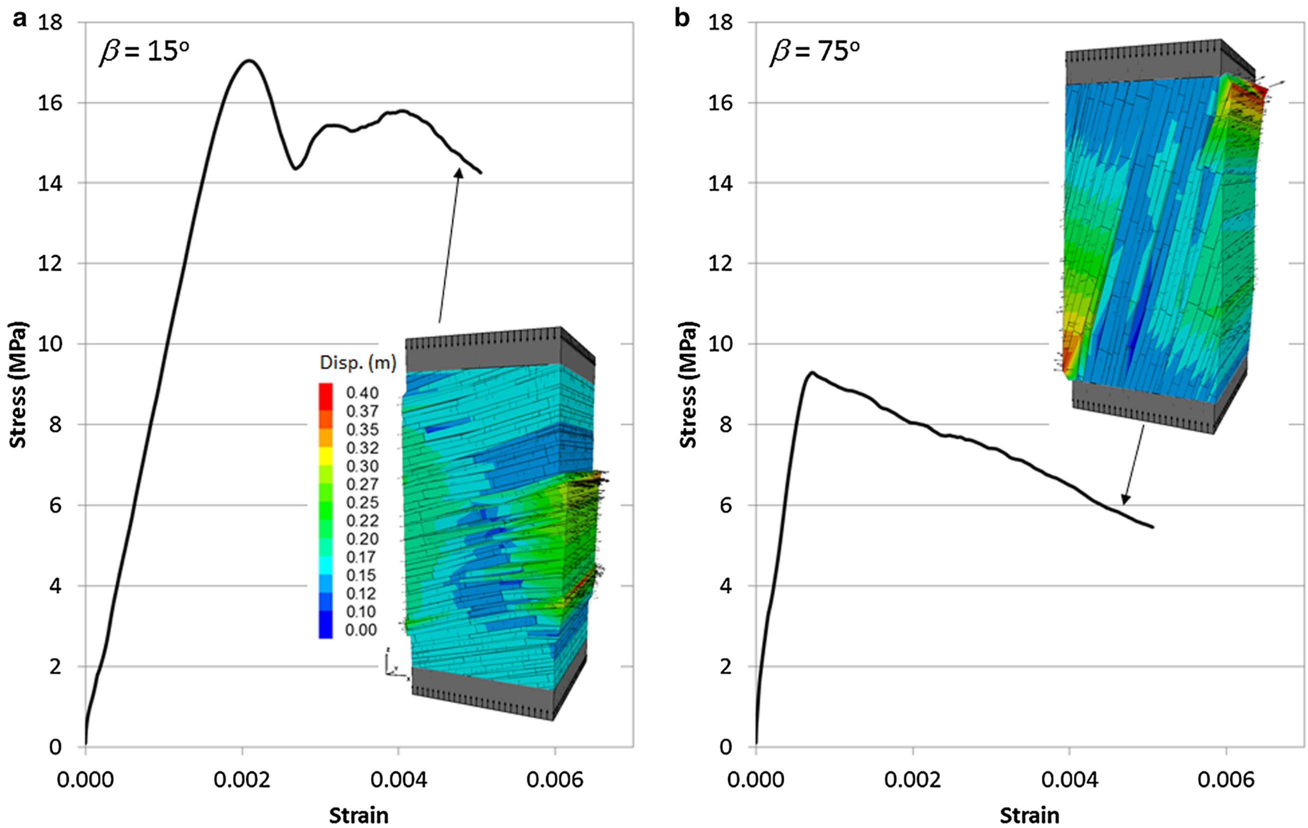

Fig. 20 UCS stress–strain response of inter-bedded sandstone, siltstone and shale rock mass at β angles of 15° and 75°

Fig. 21 Anisotropic strength of three-dimensional discontinuum and calibrated Subiquitous model

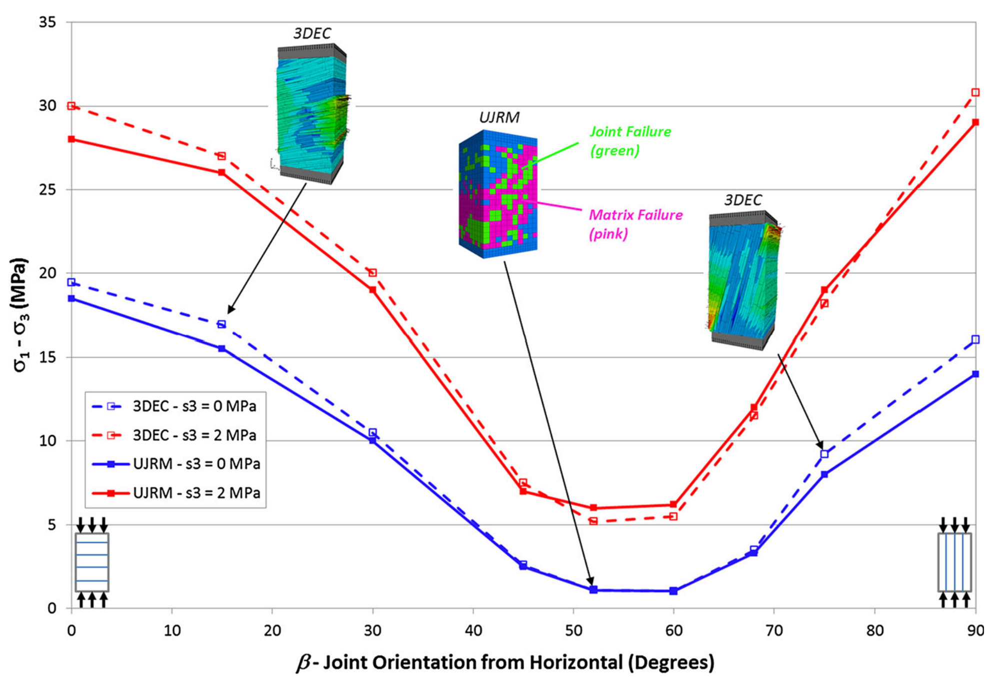

confined state. This results in less displacement and a shallower depth of bedding parting slip/separation.

It is also interesting to note in this case that when the principal stress directions were swapped (rotated 90°) little difference in the simulated damage was observed. This suggests that, in the case of anisotropic rock masses, that the direction of unloading (or decrease in stress) is more important than the maximum stress direction.

Table 7 Calibrated Subiquitous mechanical properties

Matrix properties						ubiquitous-joint properties			
E (GPa)	*v*	*c* (MPa)	ϕ (°)	σ_t (MPa)	ϵ_{crit}^{ps} (%)	c (MPa)	ϕ (°)	σ_t (MPa)	ϵ_{crit}^{ps} (%)
7.9	0.25	1.52	47	0.15	0.021	0.02	18	0	0.021

Table 8 Summary of calibrated subiquitous mechanical properties and their derivation

Matrix	
Deformation modulus	10% of intact modulus measured in laboratory
Poisson ratio	0.25 based on Hoek et al. (1995)
Cohesion	50% intact value estimated from HB strength criteria with GSI 100
Tension	10% matrix cohesion
Friction (°)	45° based on fully bulked and intact value
ϵ_{crit}^{ps}	0.016 based on Sainsbury (2012) and scaled for zone size
Joint	
Cohesion	20 kPa based on observed values (Tables 4, 5)
Friction	18° based on observed values (Tables 4, 5)
Tension	0
ϵ_{crit}^{ps}	0.016 based on Sainsbury (2012) and scaled for zone size

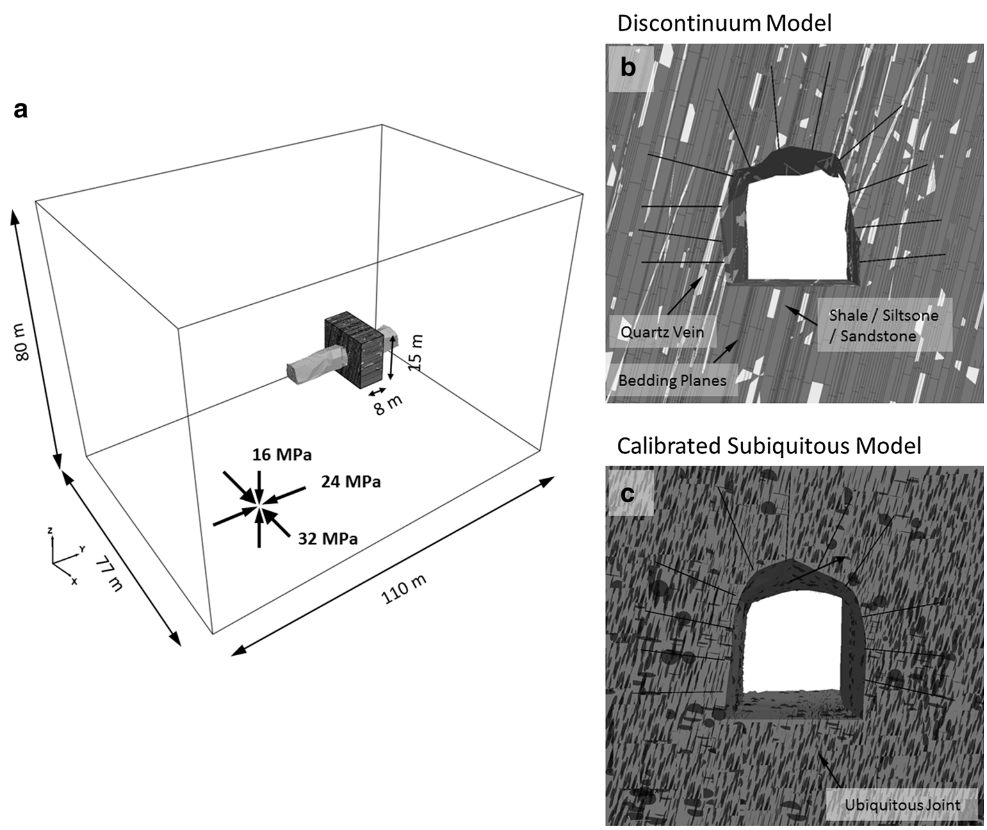

Fig. 22 Tunnel-scale model

8 Discussion of Uncertainties and Limitations

Artificial kink bands in Ubiquitous-Joint models were first reported by Cundall and Fairhurst (1986). The formation of kink bands and kink folds are common structures in thin-bedded sedimentary and foliated rocks. Due to the inability of the ubiquitous-joint formulation to represent joint spacing and bending resistance, kink band formation will always be more pronounced in Ubiquitous-Joint models.

Other failure mechanisms that involve layer bending, such as slope toppling and roof deflection, require careful

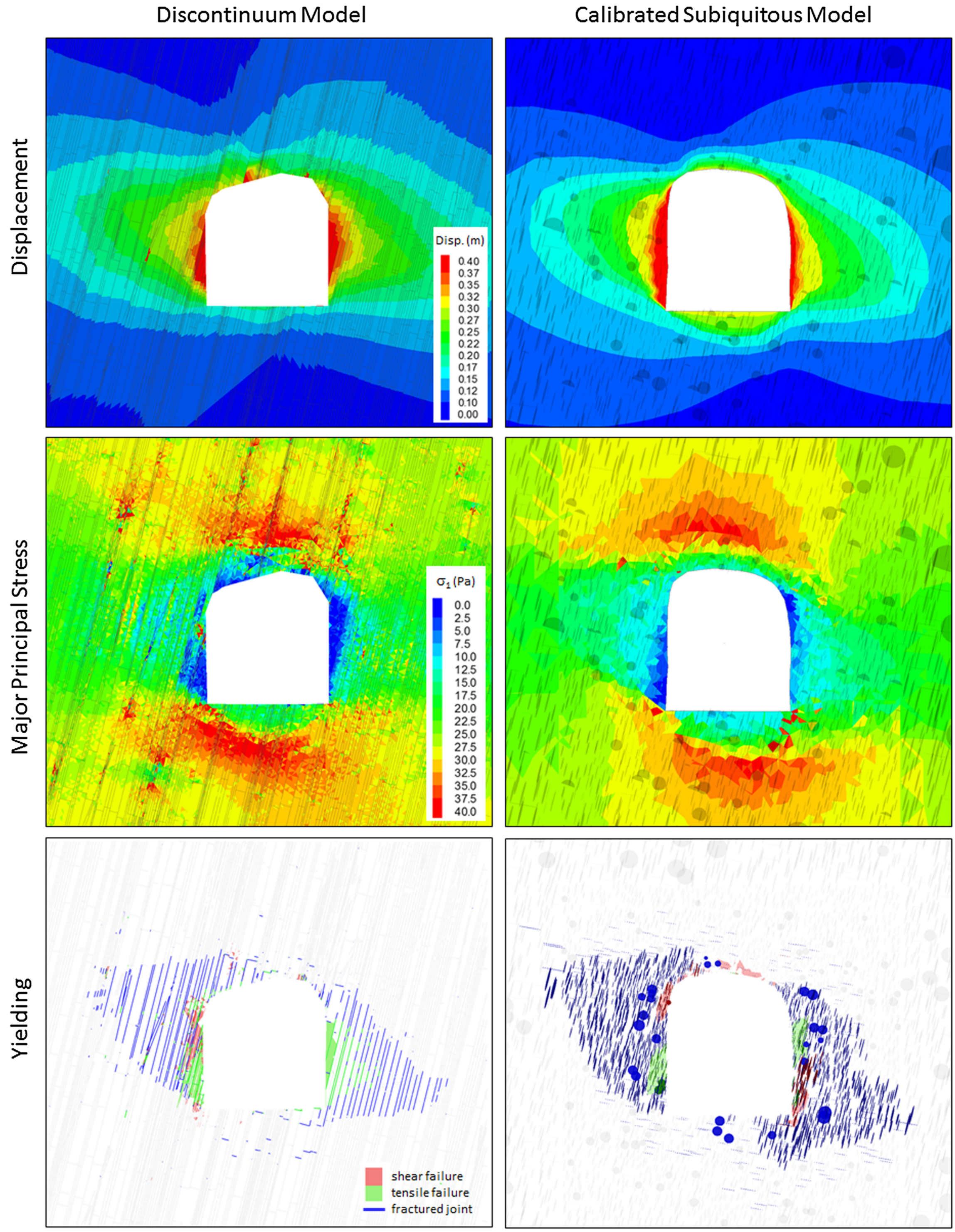

Fig. 23 Comparison of discontinuum and calibrated subiquitous sliding response

consideration in a Ubiquitous-Joint model. Sainsbury and Sainsbury and Sainsbury (2013) have previously shown how block toppling, sliding and non-daylighting wedge failures can all be simulated with a calibrated Subiquitous model; however, it is advisable to conduct parallel discontinuum analyses of such mechanisms to ensure meaningful results are achieved.

There is uncertainty as to the effects of zone size on scale effects within Ubiquitous-Joint or Subiquitous models. Care should be taken to ensure consistent unit-aspect

Fig. 24 Model geometry

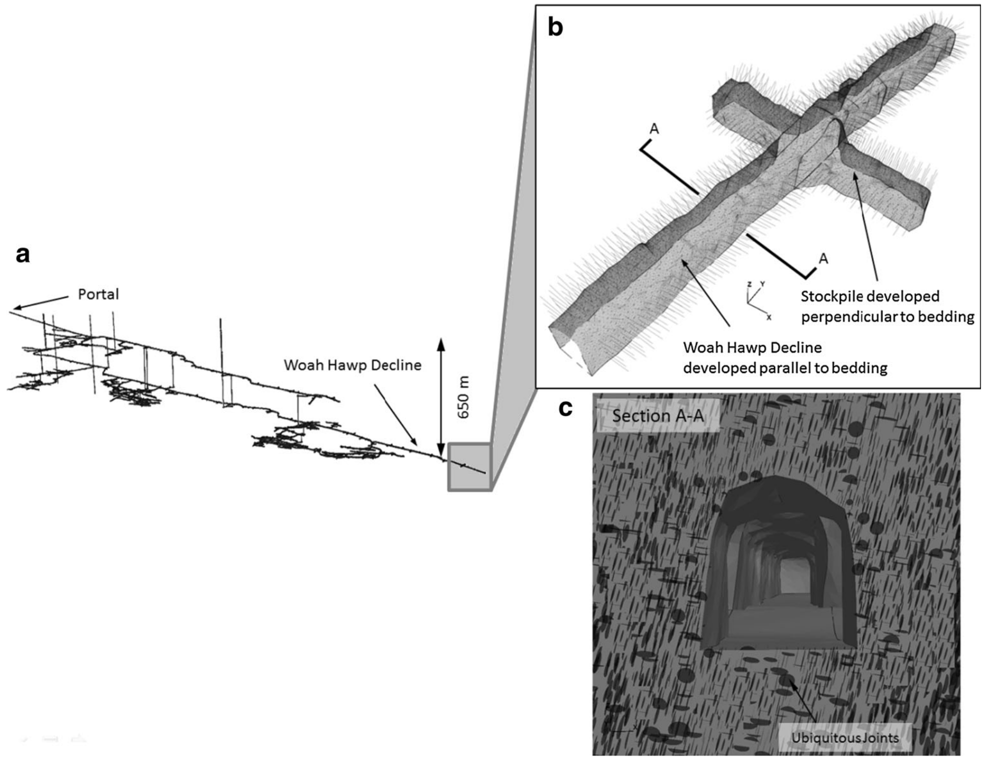

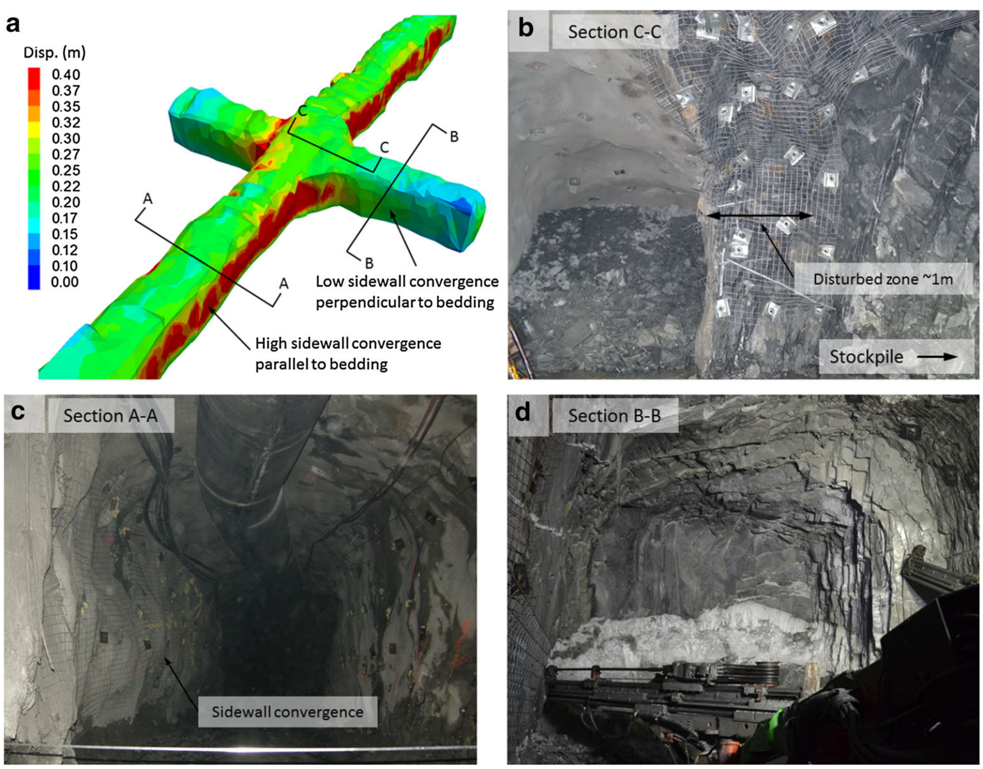

Fig. 25 Anisotropic rock mass deformation in the Woah Hawp decline

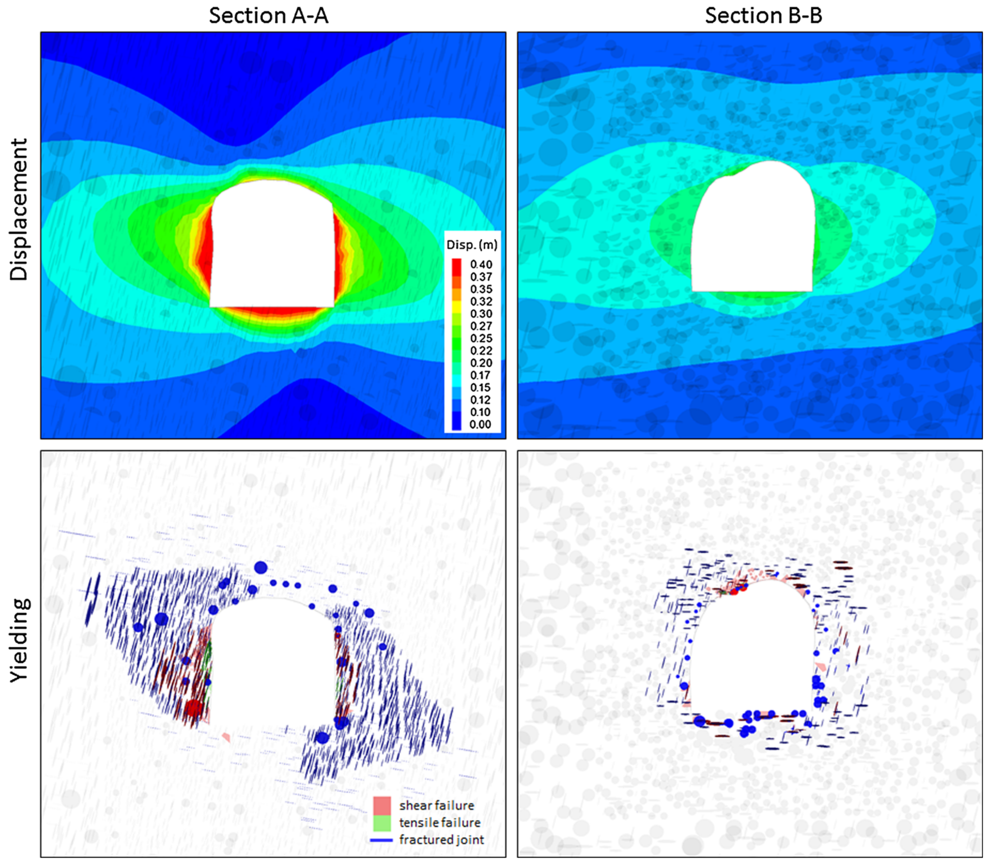

Fig. 26 Sections through model at locations A–A parallel to bedding and B–B perpendicular to bedding

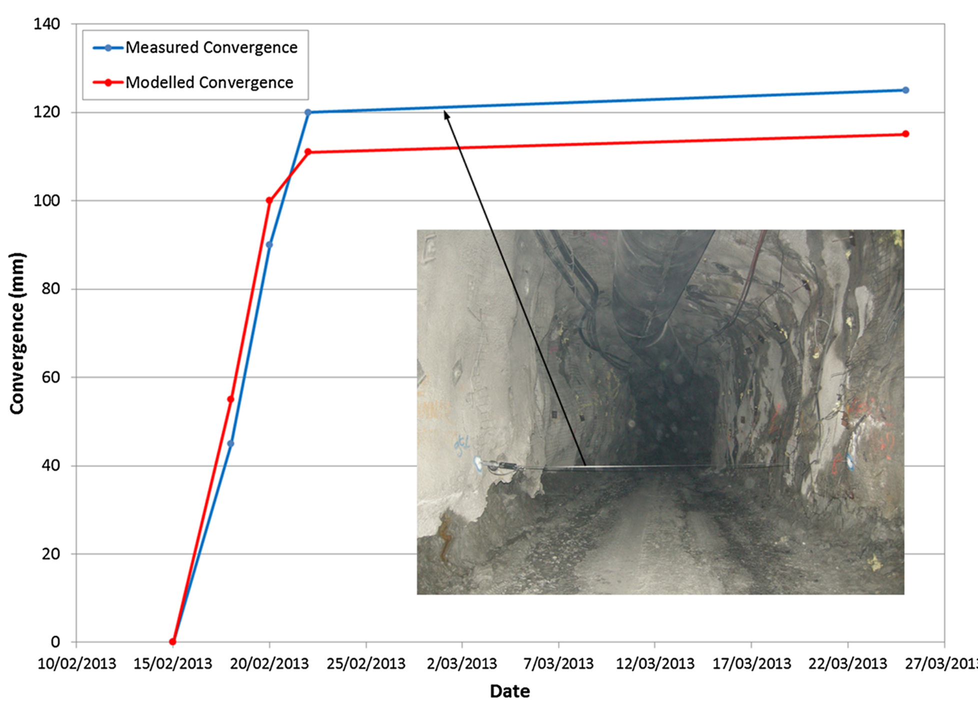

Fig. 27 Measured and simulated convergence at section A–A within the Woah Hawp decline

ratio zones sizes (i.e., the same dimension in all directions) are used in both simulated laboratory experiments and large-scale analyses.

9 Conclusion

The Ubiquitous-Joint models outlined herein show that without careful calibration of the matrix and ubiquitous-joint parameters, and consideration of the ubiquitous-joint formulation, misleading results can be obtained.

Discontinuum analyses will always provide the most rigorous assessment of anisotropic rock mass strength and deformation behavior. However, when large-scale analysis of anisotropic rock masses dictates the need for a continuum-based Ubiquitous-Joint or Subiquitous model, careful calibration of the material response to a series of discontinuum numerical experiments provides significant insight, understanding and confidence in the modeling results. The use of the more efficient calibrated subiquitous modeling technique allows robust large-scale (regional) modeling of excavation response to be conducted without complex sub-modeling routines (eg. Perman et al. 2011) having to be performed.

Acknowledgements The authors would like to thank the management team at Castlemaine Goldfields Limited for their permission to publish this work. We would also like to acknowledge the assistance of Christine Detournay (Itasca Consulting Group) for her constructive review of the paper.

References

Adhikary DP (2010) Shortcomings in the standard continuum based implicit joint model of layered rocks. J Geol Min Res 2(2):23–28

Al-Harthi AA (1998) Effect of planar structures on the anisotropy of Ranyah sandstone, Saudi Arabia. Eng Geol 50:49–57

Board M, Chacon E, Varona P, Lorig L (1996) comparative analysis of toppling behaviour at chuquicamata open—pit mine, Chile. Trans Inst Min Metall A 105:A11–A21

Brady BHG, Brown ET (2004) Rock mechanics for underground mining, 3rd edn. Springer, New York

Brown ET, Richards LR, Barr MV (1977) Shear strength characteristics of delabole slates. In: Proceedings of conference rock engineering, Univ Newcastle upon Tyne

Cai M, Kaiser PK, Tasaka Y, Minami M (2007) Determination of residual strength parameters of jointed rock masses using the GSI system. Int J Rock Mech Min Sci 44:247–265

Clark I (2006) Simulation of rock mass strength using ubiquitous-joints. In: Hart R, Varona P (eds) Proceedings of 4th international FLAC symposium on numerical modeling in geomechanics—2006, Madrid, Spain. Paper no. 08–07, Minneapolis, Itasca

Cundall PA, Fairhurst C (1986) Correlation of discontinuum models with physical observations—an approach to the estimation of rock mass behavior. Felsbau 4:4

Damjanac B, Board M, Lin M, Kicker D, Leem J (2007) Mechanical degradation of emplacement drifts at Yucca Mountain—a modeling case study part II: lithophysal rock. Int J Rock Mech Min Sci 44:368–399

Dawson EM, Cundall PA (1992) Cosserat plasticity for modeling layred rock. In: Proceedings, ISRM regional conference on fractured and jointed rock masses (Lake Tahoe, June 1992), vol 2. Lawrence Berkeley Laboratory, Berkeley, pp 269–276

Dawson EM, Cundall PA (1996) Slope stability using micropolar plasticity. In: Aubertin M et al (eds) Rock mechanics tools and techniques (2nd North American Rock mechanics symposium, Montréal, June 1996), vol 1. Balkema, Rotterdam, pp 551–558

Donath FA (1972) Effects of cohesion and granularity on deformational behavior of anisotropic rock. Studies in mineralogy and precambrian geology. Geol. Soc. Am Memoir 135:95–128

Fairhurst C, Damjanac B, Brandshaug T (2006) Rock mass strength and numerical experiments. In: Publications of the geotechnical institute no. 2006-5 (Proceedings, 35 Geomechanics Colloquium, November 2006). Technical University Mining Academy Freiberg, Freiberg, pp 1–20

Gao FQ, Stead D (2014) The application of a modified Voronoi logic to brittle fracture modelling at the laboratory and field scale. Int J Rock Mech Min Sci 68:1–14

Hoek E, Brown ET (1980) Underground excavations in rock. Institution of Mining and Metallurgy, London

Hoek E, Kaiser PK, Bawden WF (1995) Support of underground excavations in hard rock. Balkema, Rotterdam, p 215

Itasca Consulting Group, Inc. (2007) 3DEC—3-dimensional distinct element code, version 4.1. Itasca, Minneapolis

Itasca Consulting Group, Inc. (2011) UDEC—universal distinct element code, version 5.0. Itasca, Minneapolis

Itasca Consulting Group, Inc. (2012) FLAC^{3D}—fast lagrangian analysis of continua in three-dimensions, version 5.0. Itasca, Minneapolis

Jaeger JC (1960) Shear failure of anisotropic rocks. Geol Mag 97:65–72

Jaeger JC, Cook NGW (1976) Fundamentals of rock mechanics, 3rd edn. Chapman and Hall, New York

Kale SM, Trudinger JP (1975) Slope stability investigations at the Mt. Whaleback iron ore mine, Western Australia. In: Papers presented at the SA conference 1975. Part B: Whyalla, Leigh Creek, and Adelaide. AusIMM, B, pp 571–583

Karampinos E, Hadjigeorgiou J, Hazzard J, Turcotte P (2015) Discrete element modelling of the buckling phenomenon in deep hard rock mines. Int J Rock Mech Min Sci 80:346–356

Leitner R, Potsch M, Schubert W (2006) Aspects on the numerical modeling of rock mass anisotropy in tunneling. Felsbau 24:2

McLamore R, Gray KE (1967) The mechanical behavior of anisotropic sedimentary rocks. J Energy Ind Trans Am Soc Mech Eng Ser B 89:62–73

Mühlhaus HB (1993) Continuum models for layered and blocky materials. In: Comprehensive rock mechanics, Pergamon Press, pp 209–230

Perman F, Sjoberg J, Dahner C (2011) Detailed three-dimensional stress analysis of complex orebody geometry—model setup and results for the Malmberget Mine. In: Sainsbury, Hart, Detournay, Nelson (eds) Continuum and distinct element numerical modeling in geomechanics—2011. Paper: 02-04, Itasca International Inc., Minneapolis. ISBN: 978-0-9767577-2-6

Riahi A, Curran JH (2008) Application of Cosserat continuum approach in the finite element shear strength reduction analysis of jointed rock slopes. In: Geomechanics in the emerging social & technological age (CD proceedings, 12th IACMAG conference, Goa, India, October 2008), paper no. A15. X-CD Technologies Inc, Toronto

Riahi A, Curran JH (2009) Full 3D finite element Cosserat formulation with application in layered structures. Appl Math Model 33(8):3450–3454

Sainsbury B (2012) A model for cave propagation and subsidence assessment in jointed rock masses. A Thesis submitted to The

University of New South Wales in fulfilment of the requirements for the degree Doctor of Philosophy, August 2012

Sainsbury D, Sainsbury B (2013) Three-dimensional analysis of pit slope stability in anisotropic rock masses. In: Proceedings of slope stability 2013, Brisbane, Australia

Sainsbury B, Pierce M, Mas Ivars D (2008) Analysis of caving behavior using a synthetic rock mass (SRM)—ubiquitous-joint rock mass (UJRM) modeling technique. In: Proceedings of the 1st southern hemisphere international rock mechanics symposium (SHIRMS), September, 2008

Sainsbury D, Sainsbury B, Sweeney E (2016a) Three-dimensional analysis of complex anisotropic slope instability at MMG's century mine. Min Technol. doi:10.1080/14749009.2016.1163918

Sainsbury D, Sainsbury B, Paetzold H-D, Lourens P, Vakili A (2016b) Cave propagation and subsidence behaviour of lift 1 at the Palabora block cave mine. In: Seventh international conference & exhibition on mass mining—MassMin Sydney 2016

Salcedo DA (1983) Macizos Rocosos: Caracterización, Resistencia al Corte y Mecanismos de Rotura. In: Proceedings of 25 Aniversario Conferencia Soc. Venezolana de Mecánica del Suelo e Ingeniería de Fundaciones, Caracas, pp 143–172

Singh J, Ramamurth T, Venkatappa RG (1989) Strength anisotropies in rocks. Indian Geotech J 19(2):147–166

Tien YM, Kuo MC, Juang CH (2006) An experimental investigation of the failure mechanism of simulated transversely isotropic rocks. Int J Rock Mech Min Sci 43:1163–1181

Yoshinaka R, Osada M, Park H, Sasaki T, Sasaki K (2008) Practical determination of mechanical design parameters of intact rock considering scale effect. Eng Geol 96:173–186